Ecological Informatics 92 (2025) 103426

Contents lists available at ScienceDirect

Ecological Informatics

journal homepage: www.elsevier.com/locate/ecolinf

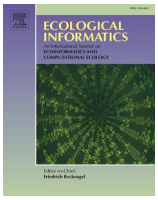

Field spectroscopy and machine learning successfully predict grassland forage quality and quantity across climate zones

Florian A. Männer [a,b,c,*], Javier Muro [d], Olena Dubovyk [e], Jessica Ferner [f], Reginald Tang Guuroh [b,g,h], Nichola M. Knox [i,j], Sebastian Schmidtlein [k], Anja Linstädter [b]

[a] University of Bonn, Institute of Crop Science and Resource Conservation, Karlrobert-Kreiten-Str. 13, 53113 Bonn, Germany
[b] University of Potsdam, Biodiversity Research/Systematic Botany, Maulbeerallee 1, 14469 Potsdam, Germany
[c] Fraunhofer-Institute for Computer Graphics Research IGD, Competence Center Bioeconomy, Joachim-Jungius-Str. 11, 18059 Rostock, Germany
[d] IE University, School of Science and Technology, Paseo de la Castellana, 259, 28046, Madrid, Spain
[e] University of Hamburg, Institute of Geography, Bundesstraße 55, 20146 Hamburg, Germany
[f] University of Bonn, Center for Remote Sensing and Land Surfaces (ZFL), Genscherallee 3, 53113 Bonn, Germany
[g] CSIR-Forestry Research Institute of Ghana, P. O. Box UP 63, Kumasi, Ghana
[h] CSIR-College of Science and Technology (CCST), P. O. Box M32, Accra, Ghana
[i] Flinders University, College of Science and Engineering, Physical Sciences Building 010, Anchor Court, Bedford Park, Adelaide, Australia
[j] Downforce Technologies Ltd, London EC4N 4SA, United Kingdom
[k] Karlsruhe Institute of Technology, Institute for Geography and Geoecology (IFGG), Kaiserstr. 12, 76131 Karlsruhe, Germany

ARTICLE INFO

Keywords:
Proximal sensing
Holistic study approach
Transferability testing
West Africa
Namibia
Germany

ABSTRACT

Grasslands cover one-third of Earth's land surface and are essential for livestock forage provision. Monitoring forage biomass and quality is key for sustainable management. Hyperspectral remote sensing and field spectroscopy is promising, but global models often fail across biomes.

We compiled data from temperate, humid tropical, and dry subtropical grasslands in Europe and Africa, spanning local growing seasons and management gradients. Using machine-learning models, we assessed the performance and transferability of global and regional predictions for forage quality (metabolizable energy), and quantity (aboveground biomass), and their combined proxy (metabolizable energy yield).

Random forest regression performed best for metabolizable energy (nRMSE = 0.108, R^2 = 0.68), aboveground biomass (nRMSE = 0.145, R^2 = 0.53), and metabolizable energy yield (nRMSE = 0.153, R^2 = 0.58). Neural networks showed highest global-to-regional transferability (nRMSE as low as 0.083), while globally trained partial least squares models outperformed regional ones (ΔnRMSE: −0.211 to 0.037). Forage quality was predicted most accurately, likely due to consistent variation in plant functional traits and strong spectral correlations. In contrast, forage quantity was harder to model due to region-specific canopy structure and pigment differences. No method achieved full spatial transferability.

Our findings highlight both the potential and limitations of hyperspectral models for forage monitoring, particularly the consistent accuracy of forage quality predictions and the superior performance of random forest models. Transferability across regions was only feasible when models accommodated local variability. Expanding spectral datasets, advancing sensors, and refining models may improve predictions, supporting more sustainable grassland management worldwide.

1. Introduction

1.1. Agronomic and ecological relevance of grasslands' forage quantity and quality

Grasslands are among the world's major ecosystems, covering approximately one-third of Earth's terrestrial surface (Gibson, 2009; Soliveres et al., 2015; White et al., 2000). Semi-natural grasslands play a critical role for agricultural production in providing forage for livestock (Bengtsson et al., 2019; Lemaire et al., 2011). Forage provision encompasses two fundamental components: quantity, typically expressed as aboveground biomass, and quality, often quantified as metabolizable

* Corresponding author.
E-mail address: florian.maenner@igd-r.fraunhofer.de (F.A. Männer).

https://doi.org/10.1016/j.ecoinf.2025.103426
Received 27 April 2025; Received in revised form 1 August 2025; Accepted 9 September 2025
Available online 11 September 2025

energy content (Ferner et al., 2018; Pavlů et al., 2006; Tirfessa and Tolera, 2020). Sustainable grassland management requires a clear understanding of both components and their spatial and temporal variation (Squires et al., 2018; Tong et al., 2019). Beyond their agronomic relevance, forage quality and quantity also serve as indicators of ecological condition, linking grassland functioning to frameworks such as ecosystem services. Aboveground biomass is widely used to estimate aboveground net primary production (Ruppert and Linstädter, 2014), a central proxy of ecosystem functioning (Maestre et al., 2022; Ruppert et al., 2015). Forage quality, in turn, is closely associated with the biochemical and structural properties of plants, particularly their metabolizable energy content (Finch et al., 2002; Getachew et al., 1998). Metabolizable energy integrates key nutritional indicators, notably fibre and protein content, which reflect plant functional strategies along gradients of resource acquisition, growth, and defence. High protein levels are characteristic of fast-growing, acquisitive species, while high fibre content indicates structural investment and persistence (Lee, 2018). These traits align with global trait frameworks such as the Leaf Economics Spectrum (Wright et al., 2004) and the multidimensional trait space described by Díaz et al. (2016), and are especially relevant in grasslands, where forage traits influence herbivory, nutrient cycling, and ecosystem processes (Díaz et al., 2007; Garnier et al., 2015). The product of forage quantity and quality – referred to as metabolizable energy yield – provides an integrative proxy of forage supply (Niemeläinen et al., 2001; Utz et al., 1994). It can not only inform grassland management decisions (Ferner et al., 2018; Guuroh et al., 2018) but also captures grassland multifunctionality by linking plant functional strategies to the provisioning ecosystem service of forage supply (Blaix et al., 2023; Michaud et al., 2015).

1.2. Hyperspectral measurement of forage quality and quantity

Understanding spatio-temporal patterns in grasslands' forage provision requires accurate and efficient monitoring of both forage quantity and quality (Amputu et al., 2024; Ferner et al., 2015; van Oudtshoorn, 2016). However, traditional methods of assessing aboveground biomass and metabolizable energy – and, by extension, metabolizable energy yield – are often expensive and time-consuming, relying on extensive fieldwork and laboratory analyses (Ferner et al., 2015). In recent years, remote sensing has emerged as a powerful alternative for estimating herbaceous biomass and forage quality. A wide range of remote sensing technologies, including satellite, airborne, and unmanned aircraft system imagery, equipped with visible light, multispectral, and hyperspectral sensors, are now being used to support these assessments (Amputu et al., 2023; Lyu et al., 2022; Marino et al., 2024; Oliveira et al., 2020; Royimani et al., 2022; Wang et al., 2022).

Among the above mentioned technologies, hyperspectral sensing shows particular promise for analysing grassland productivity and quality (Fernández-Habas et al., 2022; Ferner et al., 2015; Knox et al., 2010; Knox et al., 2011; Knox et al., 2012; Ningthoujam et al., 2025). It can determine the chemical composition of forage, including protein, fibre, and mineral content, thus allowing the prediction of metabolizable energy (Féret et al., 2021; Fernández-Habas et al., 2022; Ferner et al., 2015). While methods that are directly addressing the 3D structure of grassland canopies, like capturing object heights from overlapping airborne or spaceborne images ("structure-from-motion") or laser based sensors (e.g. LiDAR), are gaining importance (Bazzo et al., 2023; Cunliffe et al., 2016), spectrally measurable proxies for estimating aboveground biomass such as chlorophyll content per area or overall photosynthetic activity are commonly used (Mutanga and Skidmore, 2004). These methods have been successfully applied to various grassland ecosystems, including South African savanna grasslands (Singh et al., 2017), temperate ryegrass canopies (Smith et al., 2019; Smith et al., 2020), and Mediterranean grasslands (Fernández-Habas et al., 2022). Hyperspectral measurements have also been used to predict aboveground biomass in Tibetan alpine grassland (Meyer et al., 2017), and both forage quality and quantity in West African savanna grasslands (Ferner et al., 2018; Ferner et al., 2021). Application thus spans across various climate zones, including temperate, humid tropical, and dry subtropical regions.

1.3. Prediction models across climate zones

While models for forage quality and quantity cover many regions, their transferability across regions with different climate, soil, and vegetation is difficult (Schweiger et al., 2015; Yates et al., 2018). The challenge for aboveground biomass prediction, on the one hand, is often based on capturing the full range of biomass amount or physical saturation effects (Wachendorf et al., 2018; Wengert et al., 2022). On the other hand, forage quality models are not strictly based on physical principles: The compounds affecting forage quality cannot always be directly identified in reflectance data (Fernández-Habas et al., 2022; Ferner et al., 2015; Liu et al., 2021b). Instead, these models often rely on proxies that are not exclusively linked to forage quality but are influenced by environmental variables such as temperature, precipitation, and soil conditions (Wenger and Olden, 2012; Yates et al., 2018).

On top of the natural variation, local management practices, such as the frequency and intensity of grazing and mowing, vary considerably within and between regions (Blüthgen et al., 2012; Herzog et al., 2006; Vellinga and Andre, 1999). These variations further complicate the reliance on proxies in remote sensing models (Liu et al., 2021b). Consequently, models trained in a specific region and based on specific proxies often fail to account for the complexities of another, introducing biases and inaccuracies when applied elsewhere (Chen et al., 1997; Delegido et al., 2011; Roy et al., 2014). This raises the critical question whether models can be developed to accurately predict forage quality and quantity without relying on these proxies. This would enable their application across diverse and even unsampled regions, including remote areas.

The choice of modelling approach has a major impact on the accuracy of predictions from remote sensing data. Neural networks, ensemble learning and a range of statistical models employed to predict biophysical and biochemical canopy traits. Deep learning methods, such as convolutional neural networks, are characterized by capturing complex, non-linear relationships in the data, but require large amounts of high-quality training data (Bera et al., 2022). Random forest regressions are ensemble models in which predictions from multiple decision trees are used to fit models, while statistical models such as partial least squares regression provide excellent results in situations with noisy data and with a high number of predictors relative to the number of observations, as is often the case in hyperspectral remote sensing (Cook and Forzani, 2021).

Given the state of research described above, the knowledge gap remains as to the transferability and accuracy with which forage quality and quantity in grassland can be predicted from hyperspectral measurements across climate zones using a single prediction model compared to region-specific models. Within this gap, it is also not known how different learning algorithms perform in this task and with what accuracy they can be applied in different and even unsampled regions.

1.4. Objectives

This study aims to predict forage quantity and quality proxies – specifically aboveground biomass (AGB) metabolizable energy content (ME) and metabolizable energy yield (MEY) – using hyperspectral canopy reflectance data from grassland communities across various climatic zones. These zones also differ in abiotic environmental conditions, vegetation characteristics, and management practices. Specifically, we seek to:

1. Assess the accuracy of hyperspectral-based prediction models for ME, AGB, and MEY across humid tropical, dry subtropical, and temperate climate zones to develop a globally applicable model;
2. Compare the performance of different machine learning algorithms, including partial least squares regression, random forest regression, and convolutional neural networks, for predicting ME, AGB, and MEY; and
3. Evaluate the transferability of global models by validating them against regional models and assessing their predictive performance across different climate zones.

We hypothesize that (H1) spectral data will enable robust predictions of forage traits across grassland biomes, particularly for variables associated with consistently relevant functional plant strategies. Additionally, we propose that (H2) integrating complementary regional datasets with respect to functional traits of dominant plant species will improve the robustness of global models. Through these objectives and hypotheses, we aim to advance the understanding of both the potential and limitations of global models in predicting ME, AGB, and MEY.

2. Materials & methods

To reach the objectives, we selected study areas across several climate zones, while also incorporating regional climate and management gradients within study areas. By employing standardized protocols for hyperspectral measurements, field sampling, and laboratory analysis, we ensured the creation of a harmonized dataset. Based on that, we evaluated and compared the performance of different algorithms. Data collection spans study sites across three distinct climate zones, sampling along steep gradients of land-use intensity to capture substantial variation in abiotic conditions and vegetation characteristics. Model training utilized common machine learning algorithms, which were evaluated using a three-step test design: (1) assessing the performance of global models on the complete dataset, (2) evaluating the application of both global and regional models to regional datasets, and (3) testing the transferability of a globally trained model to new, unseen regions.

2.1. Study regions

We collected data in three study regions representing distinct grassland ecosystems (Fig. 1): A seasonally humid tropical savanna in

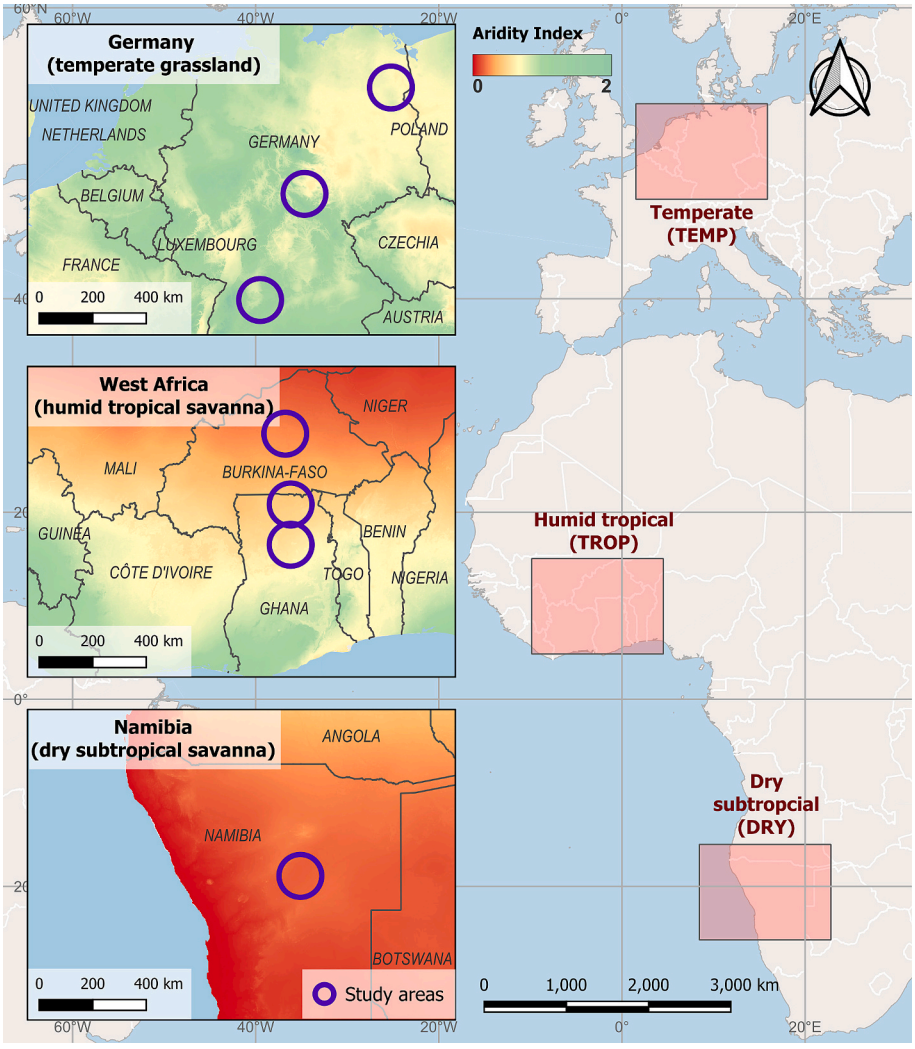

Fig. 1. Location of the seven study areas across three study regions situated in temperate (TEMP; top map), tropical (TROP; central map), and dry subtropical (DRY; bottom map) climate. The three inset maps display the aridity index within study regions, calculated using mean annual precipitation and evapotranspiration data from the WorldClim 2 dataset, as provided in Version 3 of the Global Aridity Index (Fick and Hijmans, 2017; Zomer et al., 2022). In these maps, study areas are marked by purple circles. They encompass steep gradients of local management, from which samples were collected. Map lines delineate study areas and do not necessarily depict accepted national boundaries. (For interpretation of the references to colour in this figure legend, the reader is referred to the web version of this article.)

West Africa (hereafter referred to as "TROP"), a dry subtropical thornbush savanna in Namibia ("DRY"), and temperate grasslands in Germany ("TEMP") Fig. 1. The West African savanna, classified as Sudano-Sahelian, spans northern Burkina Faso to central Ghana. It experiences a mean annual temperature (MAT) of 26–28 °C and a mean annual precipitation (MAP) of 600–1200 mm, corresponding to an UNEP aridity index (AI) from 0.31 (semi-arid) to 0.69 (humid) (Ferner et al., 2018; Guuroh et al., 2018). The nutrient-poor soils, primarily Plinthosols and Lixisols, develop on acidic metamorphic rocks (FAO, 1989) and have sand contents exceeding 80 % (Callo-Concha et al., 2013). The vegetation features a parkland savanna structure with common species such as *Vitellaria paradoxa* (Boffa, 1999). The herbaceous layer of near-natural vegetation consists of tall perennial C_4 grass species such as *Andropogon gayanus* and *Hyparrhenia involucrata* (Zerbo et al., 2018), with heights up to three meters. Livestock grazing is common, ranging from intermediate to high grazing pressures on communal rangelands (Naah et al., 2017) to low intensity in protected areas (Xu et al., 2015b).

In Namibia's dry subtropical climate zone (AI 0.14–0.16), the xeric thornbush savanna of East-Central Namibia is located within or at the edge of the Greater Waterberg Landscape. The region has a MAT from 20 to 22 °C and a MAP of 350 to 400 mm (Amputu et al., 2023; Atlas of Namibia Team, 2022). Soils are predominantly deep, nutrient-poor Arenosols derived from Kalahari sands, with sand contents exceeding 78 % (Zimmer et al., 2024). Vegetation is classified as Tree Savanna and Kalahari Woodland types (Giess, 1998). Like in West Africa, the medium-high (typically from 0.4 to 1.25 m) herbaceous layer of near-natural vegetation consists of perennial C_4 grass species; here, scattered small tuft grasses such as *Stipagrostis uniplumis*, *Aristida congesta and Eragrostis rigidior* prevail (Strohbach, 2014). The management practices in this area include rotational grazing on freehold farms and continuous grazing in communal rangelands, with low, intermediate, and high grazing pressures observed (Brinkmann et al., 2023; Zimmer et al., 2024).

The temperate grasslands in Germany, part of the German collaborative Biodiversity Exploratories project (Fischer et al., 2010), are situated in north-eastern, central, and south-western Germany. The MAT ranges from 6.5 to 8 °C, while MAP ranges from 500 to 1000 mm. The areas are underlain by Pleistocene sediments and calcareous bedrock, resulting in various soil types such as Histosols, Luvisols and Gleysols in the North-East, Cambisols, Stagnosols and Vertisols in Central Germany and Cambisols and Leptosols in the South-West (Fischer et al., 2010). Grasslands are typically treeless and dominated by stoloniferous C_3 grasses such as *Lolium perenne, Poa pratensis,* and *Alopecurus pratensis* with low (typically 0.25 to 1 m) sward heights. Management practices include the use as pastures, mown pastures, or meadows. Management intensity varies from extensive (less than three cuts or 500 animal unit days per year) to intensive (up to five cuts or 2200 animal unit days per year) (Lorenzen et al., 2024).

2.2. Data collection

2.2.1. Sampling design

We selected seven study areas across the three climate zones (Fig. 1), each characterized by a pronounced gradient from semi-natural to intensively managed grassland. In West Africa, sampling was conducted in 2012 within three study areas distributed along a regional aridity gradient, with a southern zone (aridity index: 0.45–0.63), a central zone (aridity index: 0.35–0.44), and a northern zone (aridity index: 0.23–0.30) (Fick and Hijmans, 2017; Zomer et al., 2022). Each study area covered between 10,000 and 20,000 km^2, and within these areas, sites were selected to reflect a grazing gradient, ranging from protected areas with minimal grazing pressure to heavily grazed landscapes (Guuroh et al., 2018; Xu et al., 2015a; Xu et al., 2015b). Sampling within sites followed a stratified random approach based on topographic position (Ferner et al., 2015). In Namibia, sampling took place in 2021 within a single study area of approximately 6000 km^2. Sixteen sites were selected to represent different management systems, with half located on freehold farms practising rotational grazing and the other half situated in communal lands with continuous grazing. Within each site, sampling followed local grazing gradients, ranging from very high grazing pressure near water points to moderate or low grazing pressure at maximum distances from water points (Zimmer et al., 2024).

Along these grazing gradients, nine locations were selected following a logarithmic distribution with up to three measurement plots per location, depending on site availability and shade influence. In Germany, three study areas were sampled in the years 2020 and 2021. The study areas covered between 1000 and 2000 km^2, representing a regional climate gradient across north-eastern (aridity index: 0.59–0.68), central (aridity index: 0.65–0.90) and south-western Germany (aridity index: 1.09–1.25). Within these areas, a full range from extensive to intensive local grassland management practices was sampled (Blüthgen et al., 2012). At each location, three measurements were taken (Muro et al., 2022). To account for seasonal variation, sampling across all study areas was distributed over the entire growth period. Further details on the temporal distribution of sampling events are provided in Fig. A1.

2.2.2. Hyperspectral measurements and data processing

We collected a total of 456 hyperspectral measurements from grassland canopies across the described study locations (177 measurements from Germany, 105 from West Africa, and 174 from Namibia). In Germany and West Africa, we used an ASD FieldSpec 3, while in Namibia, an ASD FieldSpec 4 Portable Spectroradiometer (ASD Inc., Boulder, CO, USA) was employed. All measurements followed a standardized protocol to ensure comparability across regions (Ferner et al., 2015). Reflectance spectra were recorded in the range of 350 to 2500 nm at a height of 1.5 m above ground in Namibia and Germany, and 1.3 m in West Africa. These heights corresponded to circular measurement areas (instantaneous field of view) of 0.36 m^2 and 0.25 m^2, respectively, which were also the defined measurement area for the respective locations. Measurements were taken from a Nadir perspective around solar noon, within a five-hour window in Germany and a six-hour window in West Africa and Namibia. Each sample consisted of 20 averaged scans per measurement, with five measurements per sample. Calibration was performed before each measurement using white reference standards (Spectralon® by LabSphere, NorthSutton, NH), pre-calibrated for each instrument. Recalibration was conducted regularly to account for atmospheric variations, and if strong or inconsistent changes were detected, the measurement was repeated.

Spectral data processing involved averaging the five replicate measurements per sample and applying a Savitzky-Golay-Filter (Savitzky and Golay, 1964) to smooth the spectra. To reduce noise, spectral regions at the sensor's upper and lower ranges (350–450 nm, 2350–2500 nm) as well as those strongly affected by atmospheric water absorption (1350–1500 nm, 1790–1990 nm) were excluded (Thenkabail et al., 2000). Data pre-processing and cleaning were conducted in R (R Core Team, 2018), using the "hsdar" package for hyperspectral data organization (Lehnert et al., 2019). The data from Germany are publicly available at the Biodiversity Exploratory Information System BExIS.

2.2.3. Field data acquisition and forage assessment

Immediately after spectral measurements, we recorded the median height of the grass layer and visually estimated bare soil cover within the exact measurement areas (Fig. 2). In Namibia and Germany, median height was estimated visually across species for the measured plot, while in West Africa, the median was calculated from the measured heights per species. Bare soil cover differed markedly across regions, with median values of 28 % in the West African tropical savanna, 35 % in the subtropical dry savanna of Namibia, and only 2 % in the temperate grasslands of Germany. Vegetation heights also differed between regions at the time of hyperspectral measurements. In the tropical savanna, herbaceous vegetation heights can reach up to 200 cm, but grazing typically

favours low-growing plants and limits height, resulting in median plant height of just 24.0 cm. In the subtropical savanna, the median height was 35.0 cm, while in the temperate grasslands it was estimated at 19.5 cm.

After recording the spectral measurements, aboveground herbaceous biomass was clipped to stubble height. Samples from West Africa and Namibia were air-dried and shipped to Germany, while those from Germany were directly oven dried. The dry weight of aboveground biomass (AGB) per unit area was determined by weighing the samples after oven-drying (55–60 °C, >48 h). The dried material was then ground to 1 mm using a cutting mill for in-vitro gas production analysis. Only samples from areas with a vegetation cover exceeding 40 % were used for these analyses to enhance the robustness of the prediction models, which restricts their applicability for ME and MEY predictions to areas with substantial vegetation cover (> 40 %). Accounting for measurement errors, losses during in-vitro gas production analysis, and sample exclusions based on vegetation cover, the final dataset included 318 ME measurements (101 from West Africa, 109 from Namibia and 108 from Germany).

For in vitro-gas production assessment, subsamples were incubated for 24 h in a medium containing sheep rumen liquid, following the method of Menke and Steingass (1988). Crude protein content was measured using two different methods: the Kjeldahl method for samples from West Africa and Germany (VDLUFA, 1976) at the Institute for Animal Science, University of Bonn, and a EA3100 CHNS-O elemental analyser (Eurovector, Pavia, Italy) at the Institute for Biodiversity Research/Systematic Botany, University of Potsdam, for the Namibian samples. ME, expressed in MJ kg^{-1} of dry matter, was then calculated as follows (Menke and Steingass, 1988):

$$ME \approx 2.2 + 0.1357*gas + 0.0057*protein + 0.0002859*protein^2 \quad (1)$$

Where gas represents the in-vitro gas production within 24 h, expressed as ml (200 mg dry matter)$^{-1}$, and protein denotes the protein content in g (kg dry matter)$^{-1}$, calculated as the measured nitrogen-content multiplied by 6.25.

From the values of ME in MJ kg^{-1} of dry matter and AGB in g dry matter m^{-2}, the amount of ME per area was calculated as MEY in MJ m^{-2}:

$$MEY = \frac{ME*AGB}{1000} \quad (2)$$

These three proxies of forage quantity (AGB), forage quality (ME) and a combination of both (MEY) were served as prediction targets, culminating in a distinct dataset for subsequent analyses of spectral canopy reflections across three climatic zones. However, it is imperative to acknowledge that variations in data collection timing, measurement geometries, and the specific spectroradiometers employed across different regions may influence both the analysis and the transferability of the resultant predictive models.

2.3. Model setup

We applied three machine learning algorithms to predict forage characteristics from spectral measurements: random forest (RF) regression, partial least squares (PLS) regression, and a one-dimensional convolutional neural network (cNN) regression. Neural networks such as cNN excel at capturing complex, non-linear relationships in data, making them particularly effective when dealing with very complex datasets (Bera et al., 2022). Their main advantage lies in their ability to learn data representations even in case of highly complex patterns (Kattenborn et al., 2021). However, they require vast amounts of high-quality training data, which limits their application in situations where training is based on time and cost intensive field measurements. Ensemble learning approaches, such as RF regression, use predictions from multiple decision trees to fit models. They are capable of handling datasets with mixed data types, noise, and outliers, and can perform well with relatively small training samples. PLS regression excels in situations with noisy data and where the number of predictors is high relative to the number of observations, as it is often the case in hyperspectral remote sensing. Especially some dedicated derivatives of PLS regressions are able to deal with non-linearity (Cook and Forzani, 2021) but they are not the best choice for highly distorted feature spaces, meaning input data with significant alterations or irregularities due to data noise, outliers or feature extraction methods. Dealing with feature space distortion is a typical use-case for machine learning.

Models of the three forage proxies were developed separately for each climatic zone (regional models) and across all zones (global models). To ensure normal distribution of residuals in PLS regression, ME was log-transformed, while AGB and MEY were transformed using the natural logarithm. Predictor creation, selection, and model setup were conducted in R (R Core Team, 2018), using the "hsdar" package for predictor creation (Lehnert et al., 2019) and the „randomForest" and "pls" packages for RF and PLS model development, respectively (Liaw and Wiener, 2022).

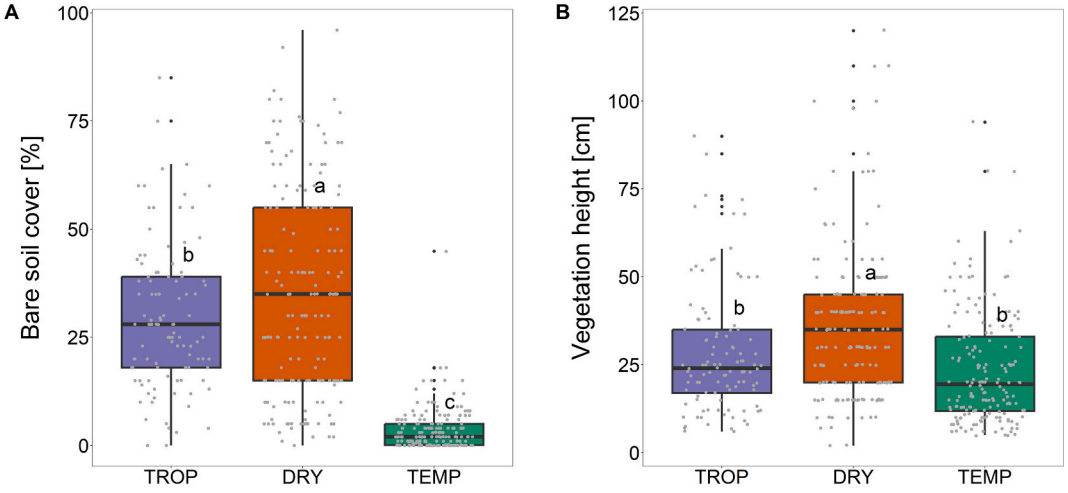

Fig. 2. Distribution of bare soil cover and vegetation height across the three study regions – West African tropical savannas (TROP; $n = 105$), Namibian dry subtropical savanna (DRY; $n = 174$), and German temperate grassland (TEMP; $n = 177$). Study regions differed in bare soil cover (A) and the vegetation height (B) which represents the height of the herbaceous vegetation layer. Letters above boxplots indicate the result of a One-way-ANOVA and Tukey test, showing significant differences in bare soil cover ($p < 0.001$) and grass height ($p < 0.001$) across study regions.

2.3.1. Predictor creation and reduction

The predictor set was mainly based on reflectance spectra, which were reduced to a spectral resolution of 10 nm, resulting in 168 predictors. Additionally, the first derivative of the spectra was calculated, yielding 153 further predictors, which can enhance spectral information extraction compared to absolute reflectance values (Knox et al., 2010). Vegetation indices as defined by Obermeier et al. (2019) and absorption features derived from segmented continuum hull removal added 170 more predictors, resulting in a total of 491 predictors. Predictor reduction for RF and PLS models in both regional and global models was conducted through a repeated backward elimination process based on predictor importance. The optimal predictor sets for both RF and PLS models were determined by minimizing mean square error (MSE) in repeated 10-fold cross validation, considering different combinations of spectra, first derivatives, absorption features, and vegetation indices. The first derivative predictor set consistently outperformed other sets across all models and were therefore selected, leading to high predictors-to-observations ratios of approximately 0.5 for ME and MEY and 0.3 for AGB (Table A 1). To maintain comparability and ensure consistency, the same predictors were applied to regional and global models, assuming that reflectance is linked to individual proxies representing recurring mechanisms (Step 2 + 3 in Fig. 3). To avoid blind predictor selection by the algorithm, the selected spectral bands were further evaluated concerning their biophysical relevance for biomass and yield, pigments, protein, and fibre contents, which should be reflected in the ME, AGB and MEY predictor sets. The cNN models also utilized the first derivative of the 153 spectral bands, as this yielded the best results for AGB and MEY, while performance for ME remained unchanged.

2.3.2. Model training and validation

For RF model training, hyperparameters were optimized by setting the number of predictors per node to the square root of the total number of predictors, while the number of decision trees was varied between 50 and 500 to determine the optimal structure. PLS regression models were trained by optimizing the number of latent vectors. For the cNN models, an optimal architecture (three inner layers, 128 nodes, and RMSprop as the optimizer) was identified using the Keras Tuner, balancing the three study parameters (O'Malley et al., 2019).

Model performance was evaluated through various test designs (Fig. 3). Accuracy was assessed for each forage proxy (ME, AGB, and MEY) and machine learning algorithm (RF, PLS, and cNN) based on the coefficient of determination (R^2) and the normalized root mean squares error (nRMSE), where normalization was performed using the minimum-to-maximum range. The accuracy of each global model was validated using 5-fold cross-validation (CV; Step 4 in Fig. 3).

To assess the transferability of a global model to a specific climate region, we compared the performance of globally and regionally trained models on regional datasets. In contrast to the previous cross-validation, regional datasets were split up into training (80 %) and test (20 %) subsets (Step 5 in Fig. 3). A new global model was trained on the combined regional training datasets and validated against the combined regional test dataset. Additionally, three regional models were trained on the single regional training datasets. Afterwards, regional test datasets were predicted using both the corresponding regional models and the global model to compare their performance on the unseen test data. A direct comparison of global and regional models was made by calculating the difference in nRMSE between them ($\Delta nRMSE$), expressed as:

$$\Delta nRMSE = nRMSE_{regional} - nRMSE_{global} \quad (3)$$

A positive $\Delta nRMSE$ indicates better precision for the global model, while a negative value suggests superior regional model performance.

To assess model transferability, a spatial cross-validation (CV) was conducted, where models trained on data from two regions were validated against data from a third region (Step 6 in Fig. 3). This process was repeated for all possible combinations of the three regions.

In summary, our test design consisted of three validation stages (Fig. 3): (1) Evaluation of models on the complete global dataset, (2) applying both globally and regionally trained models to regional datasets to assess their transferability and comparability, and (3) testing the spatial transferability of a globally trained model to new, independent regions.

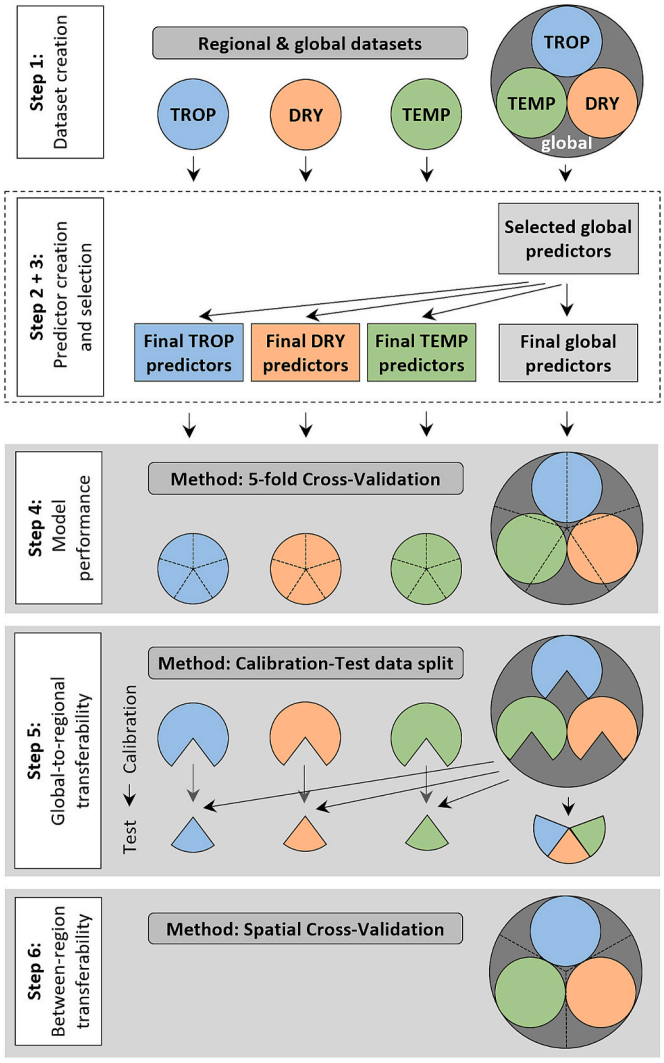

Fig. 3. Calibration and validation setup of forage proxies in six steps. Step 1 involves dataset compilation across four spatial foci. Single circles represent regional datasets from tropical (TROP), dry subtropical (DRY) and temperate (TEMP) climate zones, while the three combined circles indicate the global dataset used for model calibration and validation. Steps 2 and 3 outline predictor creation and selection, incorporating all spectral bands, their derivatives, features, and indices. Predictors are selected based on the global dataset and subsequently applied to the regional datasets. Steps 4, 5 and 6 illustrate the three validation stages: A test of model performance with the aid of a 5-fold cross-validation, a test of global-to-regional transferability via a comparison of global and regional model performances using a fixed calibration and test data split of 80 and 20 %, respectively, and an evaluation of models' between-region transferability using spatial cross-validation.

3. Results

3.1. Importance of wavelength regions in modelling

The three machine learning algorithms – random forest (RF), partial least squares regression (PLS), and neural networks (cNN) – assigned varying degrees of importance to different spectral bands. For predicting metabolizable energy content (ME), key areas in the reflectance

spectrum were associated with specific forage characteristics (Fig. 4D): chlorophyll and carotenoids between 450 and 700 nm (pigment area), biomass and yield between 700 and 1350 nm (AGB area), which also contains important water absorption bands at 900 and 1200 nm, protein absorption between 1500 and 1750 nm (protein area), and both proteins and fibre influence between 2000 and 2350 nm (fibre & protein area).

The predictor importance for ME models per learning algorithm showed quite some differences. The number of selected predictors varied across algorithms and forage proxies. The optimal RF model utilized 30 predictors spanning the visible, near-infrared, and shortwave-infrared spectra (Fig. 4B), whereas PLS regressions (Fig. 4C) and cNN models (Fig. 4D) used the full spectrum of 153 wavelengths to predict ME (Table A 2) resulting also in higher importance values per predictor for RF models. These models also exhibited greater variability in predictor importance between regional and global modelling compared to PLS models, where predictor importance remained relatively stable across models for the three study regions (Fig. 4B & C). In the final RF predictor selection using the global dataset, key wavelengths from each spectral area were well represented. However, some important wavelengths or areas for predicting ME were showing higher importance across the machine learning algorithms (Fig. 4B-D), focusing on the pigment area at 450, 550 and 670 nm, water absorption and AGB areas at 760, 850, 970 and 1180 nm, the protein area at 1660 nm and the fibre/protein area at approximately 2100 and 2280 nm.

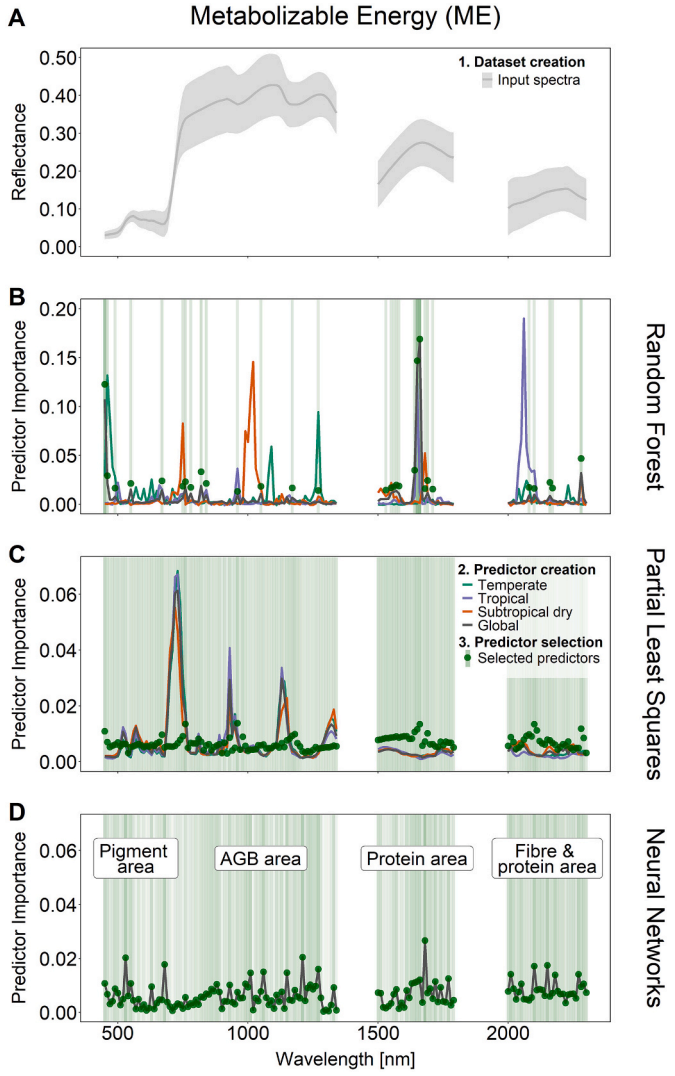

Fig. 4. Key wavelength areas for predicting metabolizable energy (ME) across different machine learning models. The figure illustrates the importance of individual wavelengths in the full hyperspectral range of 450–2350 nm (A), using the first derivative of canopy reflectance spectra for ME prediction using random forest regression (B), partial least squares regression (C), and a one-dimensional convolutional neural network (D). The grey line and light grey shading in A represent the mean and standard deviation of the raw spectral input across all regions. Coloured lines indicate predictor importance for regional models, while black lines represent global models. Green dots mark the final selected predictors, with green shading indicating their relative importance, where higher greenness intensity reflects greater importance. White labels in C denote spectral areas with characteristic absorption features: the 'pigment area' (chlorophyll and carotenoids) below 700 nm, the 'AGB area' between 700 and 1350 nm, the 'protein area' between 1500 nm and 1790 nm, and the 'fibre & protein area' from 2000 nm onwards. For additional result graphs, see Fig. A2. (For interpretation of the references to colour in this figure legend, the reader is referred to the web version of this article.)

The models for the two other forage proxies, aboveground biomass (AGB) and metabolizable energy yield (MEY) were having similar differences, while backward selection resulted in a higher selection of predictors for PLS models (Fig. A2).

3.2. Model performance

The predictive performance of global models varied significantly across forage proxies and depended on the machine learning algorithm used (Fig. 5). This was assessed by comparing the 5-fold cross-validation results (Step 4 in Fig. 3) for ME, AGB, and MEY across the three machine learning algorithms. Among the models, RF consistently achieved the highest accuracy for all forage proxies, with ME predictions being the most robust across algorithms. The RF model for ME exhibited the best overall performance, with an nRMSE of 0.108 and an R^2 of 0.676 (Fig. 5A). However, RF models tended to underestimate AGB and MEY at higher values (Fig. 5B-C), particularly above approximately 200 g/m^2 and 2.5 MJ kg^{-1}, respectively. In contrast, neural networks exhibited the lowest predictive performance across all three forage proxies (Fig. 5G-I), with the lowest accuracy of all models observed for MEY prediction (Fig. 5I).

A comparison of combined regional models per forage proxy and algorithm (Fig. 6) revealed similar performances when aggregating results across all three climatic regions. However, forage proxy values were not evenly distributed among study regions. This was particularly evident for ME, which showed higher values in the temperate region compared to the tropical and subtropical regions (Fig. 6A, D, G).

3.3. Global-to-regional transferability

To assess the transferability of a global model to a specific climate region, we compared the performance of globally and regionally trained models on regional datasets. We applied both the globally and regionally trained models to an independent test dataset which none of the models had encountered during training (Step 5 in Fig. 3).

The resulting predictions were visualized in a combined distribution graph, illustrating both overall prediction accuracy (nRMSE) and the difference in performance between the global and regional models (ΔnRMSE) (Eq. 3 & Fig. 7 A). An overview of ΔnRMSE values across all forage proxies, machine learning algorithms, and regions (Fig. 7 B) indicates that global and regional models are mostly not different to their regional counterparts. For RF and PLS models, the differences between global and regional performance were not statistically significant.

There is only a tendency visible that regional models slightly outperform global models for their respective region. The most pronounced decline in accuracy when using a global model instead of a regional one occurred for MEY prediction in the dry subtropical region using PLS (ΔnRMSE = −0.211). However, global models occasionally outperformed regional ones, with the highest positive difference observed for ME prediction in the tropical region using cNN (ΔnRMSE = 0.083).

Interestingly, global cNN models often achieved higher accuracy

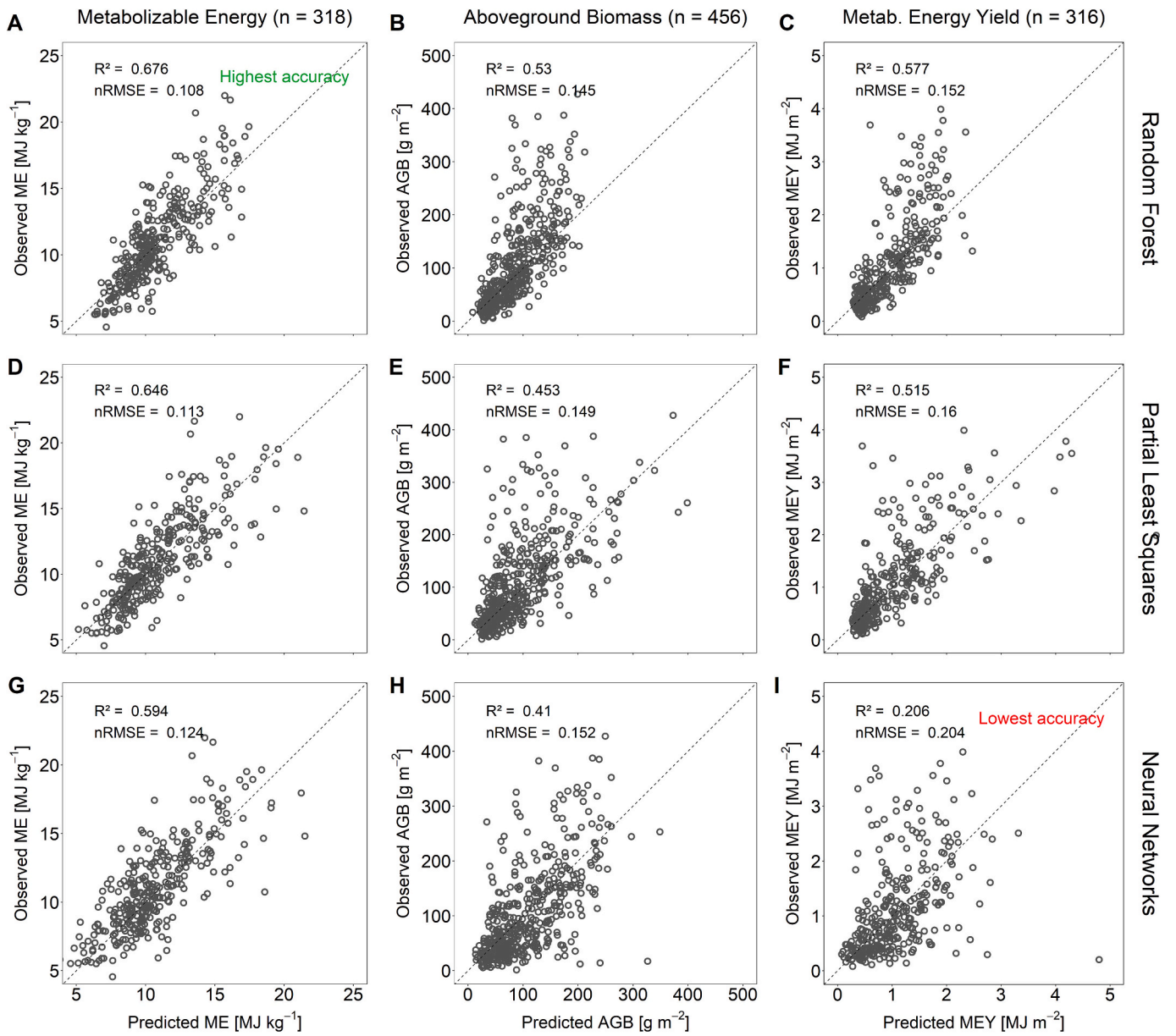

Fig. 5. Performance of global prediction models for forage traits using 5-fold cross validation across different machine learning models. Shown are validation results for metabolizable energy, aboveground biomass, and metabolizable energy yield using random forest regression (A-C), partial least squares regression (D—F) and a one-dimensional convolutional neural network regression (G-I). For a detailed comparison, including all regional and global model results, see Fig. A3.

than their regional counterparts, with ΔnRMSE values ranging from −0.032 to 0.083, showing significant improvements in the dry subtropical region. In contrast, global PLS models tended to almost consistently underperform compared to their regional counterparts, with ΔnRMSE values ranging from −0.211 to 0.037.

3.4. Between-region transferability

Spatial cross-validation, in which models were trained with data from two climatic regions and validated on data from the third region (Step 6 in Fig. 3), revealed significant differences in spatial transferability between the three forage proxies, while differences between the three machine learning algorithms were less pronounced (Fig. 8). ME models exhibited very limited spatial transferability, with nRMSE values ranging from 0.204 to 0.255 and R^2 values between 0.000 and 0.022. In contrast, AGB (nRMSE: 0.235–0.365; R^2: 0.001–0.025) and MEY (nRMSE: 0.262–0.286; R^2: 0.003–0.066) showed a certain degree of spatial transferability. However, ME model transfer resulted in systematic biases, with overestimation in the tropical region and underestimation in the temperate region. Similarly, AGB and MEY models tended to overestimate values in the tropical region, as evident from distinct point clouds in the validation dataset (Fig. 8), while predictions for the dry subtropical region were constantly underestimated.

The choice of training algorithm also influenced model transferability. RF and PLS regression produced distinct point clouds in ME analyses (Fig. 8A-F), whereas cNN predictions were more broadly distributed (Fig. 8G-I). Despite these differences, the RF model consistently performed best in spatial cross-validation across all three forage proxies.

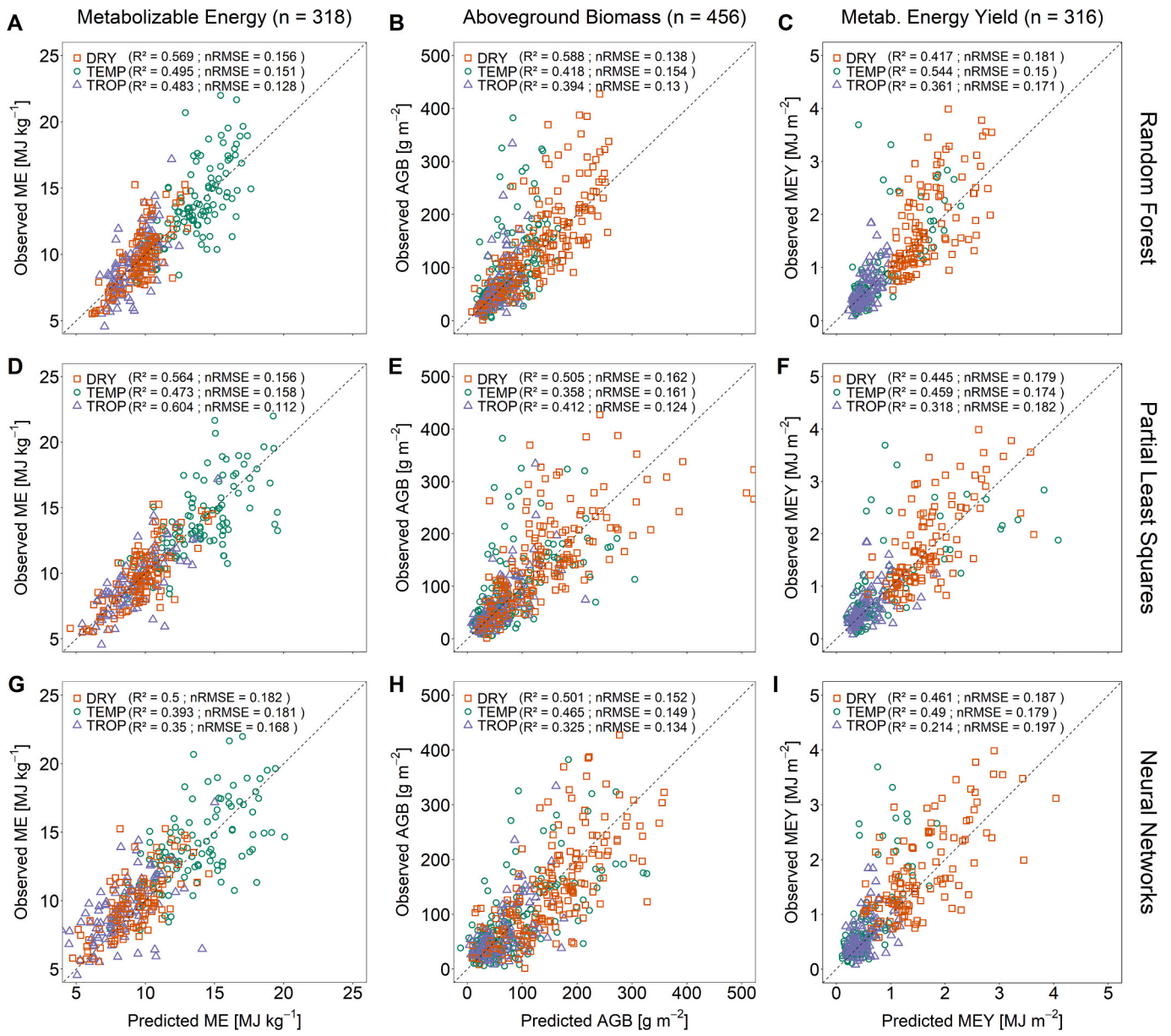

Fig. 6. Performance of combined regional prediction models per forage proxy and algorithm. Shown are the combined 5-fold cross-validation results for three forage proxies - metabolizable energy, aboveground biomass, and metabolizable energy yield - using regional models trained separately for tropical (TROP), dry subtropical (DRY) and temperate (TEMP) climate zones. Predictions were made using random forest regression (A-C), partial least squares regression (D—F), and a one-dimensional convolutional neural network regression (G-I).

4. Discussion

4.1. Development and evaluation forage prediction models

We developed globally applicable models for predicting grasslands' forage quality and quantity from hyperspectral field measurements. To our knowledge, this is the first study to create global models based on ground hyperspectral sensing and systematically compare their performances against regional models. Previous studies tested regional models through a spatial cross-validation (Killeen et al., 2024; Meyer et al., 2019; Muro et al., 2022). Achieving this required a study design with extensive standardized measurements and a rigorous validation method. To ensure broad applicability, we compiled a dataset from seven study areas across three climate zones, covering steep gradients of land-use intensity, abiotic conditions, and vegetation characteristics. Moreover, our study also covered gradients of seasonality in all study areas, allowing us to test the applicability of a global model on a regional dataset and compare them to a regionally trained model. Our study effectively captured grass species' functional strategies observable in grasslands worldwide (Da Silveira Pontes et al., 2015; Suttie et al., 2005). Hence, key functional traits influencing spectral reflectance – such as leaf structure, canopy architecture, and biochemical composition – are well-represented in the training data. Using standardized protocols for field sampling, hyperspectral measurements, and laboratory analysis, we predicted forage quality (metabolizable energy), forage quantity (aboveground biomass), and metabolizable energy yield (their combined proxy) from top-of-the-canopy reflectance spectra. We systematically evaluated the performance of three machine learning algorithms: random forest, partial least squares, and one-dimensional convolutional neural network, using a three-step testing scheme: (1) evaluating the general performance of globally trained models, (2) applying both globally and regionally trained models to regional

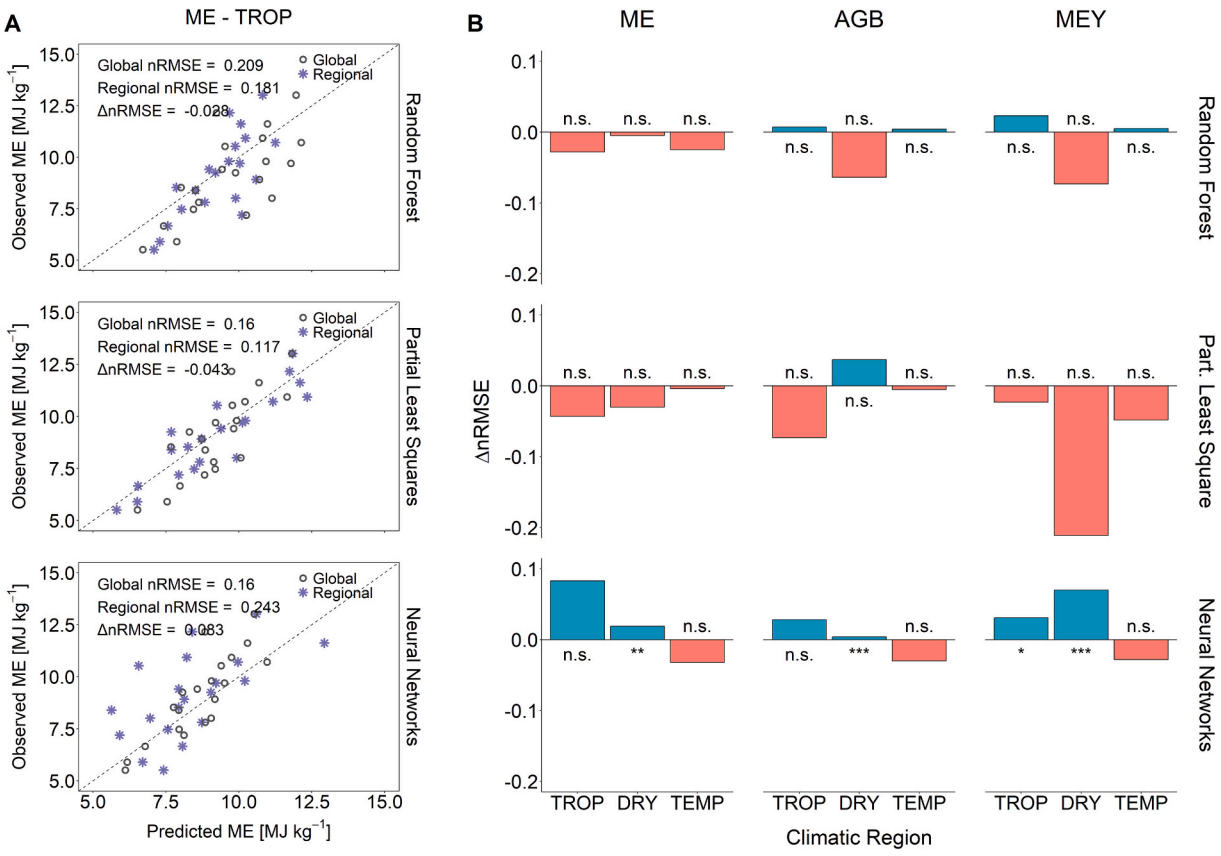

Fig. 7. Performance comparison of globally and regionally trained models on a regional dataset using different algorithms. A: Exemplary comparison of metabolizable energy (ME) prediction models: one trained on global data and one on tropical data, both evaluated on an independent tropical test dataset that neither model had encountered during training. The comparison metric used is ΔnRMSE, which represents the difference in normalized root mean square error (nRMSE) between the globally and regionally trained models (all other comparisons are shown in Fig. A4). B: Summary of all comparisons based on ΔnRMSE for the three regional models (tropical, dry subtropical, and temperate) and the three target variables (ME, aboveground biomass [AGB], and metabolizable yield [MEY]). Results are shown for the three training algorithms: random forest (RF), partial least squares (PLS), and neural networks (cNN). The significance level of the difference between global and regional model estimates, determined using a paired *t*-test, is indicated at the bottom of each bar ('***': $p < 0.001$; '**': $p < 0.01$; '*': $p \leq 0.05$; 'n.s.': $p > 0.05$).

datasets, and (3) testing the transferability of global models to regions with different climatic conditions.

4.2. Importance of wavelength regions in modelling

Our models successfully predicted forage quality and quantity across several study areas and climate zones. Forage quality was predicted more accurately than quantity when using the full spectral range. While we expected algorithm-specific variations in predictor selection, all models consistently relied on spectral bands in four key wavelength regions: 450–670 nm, 700–1350 nm, 1500–1800 nm, and 2000–2350 nm. This consistency aligns with previous findings on the functional significance of these bands: Reflectance in the visible spectrum (450–700 nm) is linked to photosynthetic and photoprotective leaf pigments, which are associated with metabolizable energy (Biewer et al., 2009; Curran, 1989; Pullanagari et al., 2012). Near-infrared reflectance (680–1350 nm) is influenced by water absorption and photon scattering caused by canopy structural properties, making it relevant for both forage quality and quantity estimation (Thenkabail et al., 2000; Thenkabail and Lyon, 2012; Zhao et al., 2023). Shortwave infrared wavelengths (1500–1800 nm and 2000–2350 nm) is, besides water absorption, driven by absorptions from proteins, and fibre compounds that are closely related to metabolizable energy (Féret et al., 2021; Ferner et al., 2015; Thenkabail and Lyon, 2012). However, algorithm-specific learning strategies, with every algorithm using idiosyncratic subsets of the specific spectral bands, prevented the identification of a universal predictor set applicable across all algorithms (Omeer and Deshmukh, 2021; Zhang et al., 2022). This also reinforces the importance of the entire hyperspectral range of vegetation reflectance for predicting both forage quality and quantity (Duranovich et al., 2020; Ferner et al., 2015; Ferner et al., 2021).

4.3. Machine learning algorithms and model performance

Among the tested algorithms, random forest consistently outperformed partial least squares regression and one-dimensional neural networks in predicting forage proxies (Fig. 5), particularly in global models where large training datasets were available. This performance advantage likely stems from the algorithm's adaptability in creating decision trees that accommodate complex data structures and high predictor-to-observation ratios – approximately 0.5 for metabolizable energy and metabolizable energy yield, and 0.3 for aboveground biomass (Evans et al., 2011; Qi, 2012). Despite this strong performance of random forest regressions, we observed a tendency toward underestimation, particularly for aboveground biomass and metabolizable energy yield. This may be caused by either a saturation effect or an unbalanced data set that favours low values, both of which support the reported difficulties of random forest to predict extreme values (Xu et al., 2016). While some studies suggested that neural networks might struggle with small datasets (Jozdani et al., 2019; Ng et al., 2022; Padarian et al., 2019b), shallow (Muro et al., 2022) and deep neural networks (Dieste et al., 2024) have been shown to perform well with

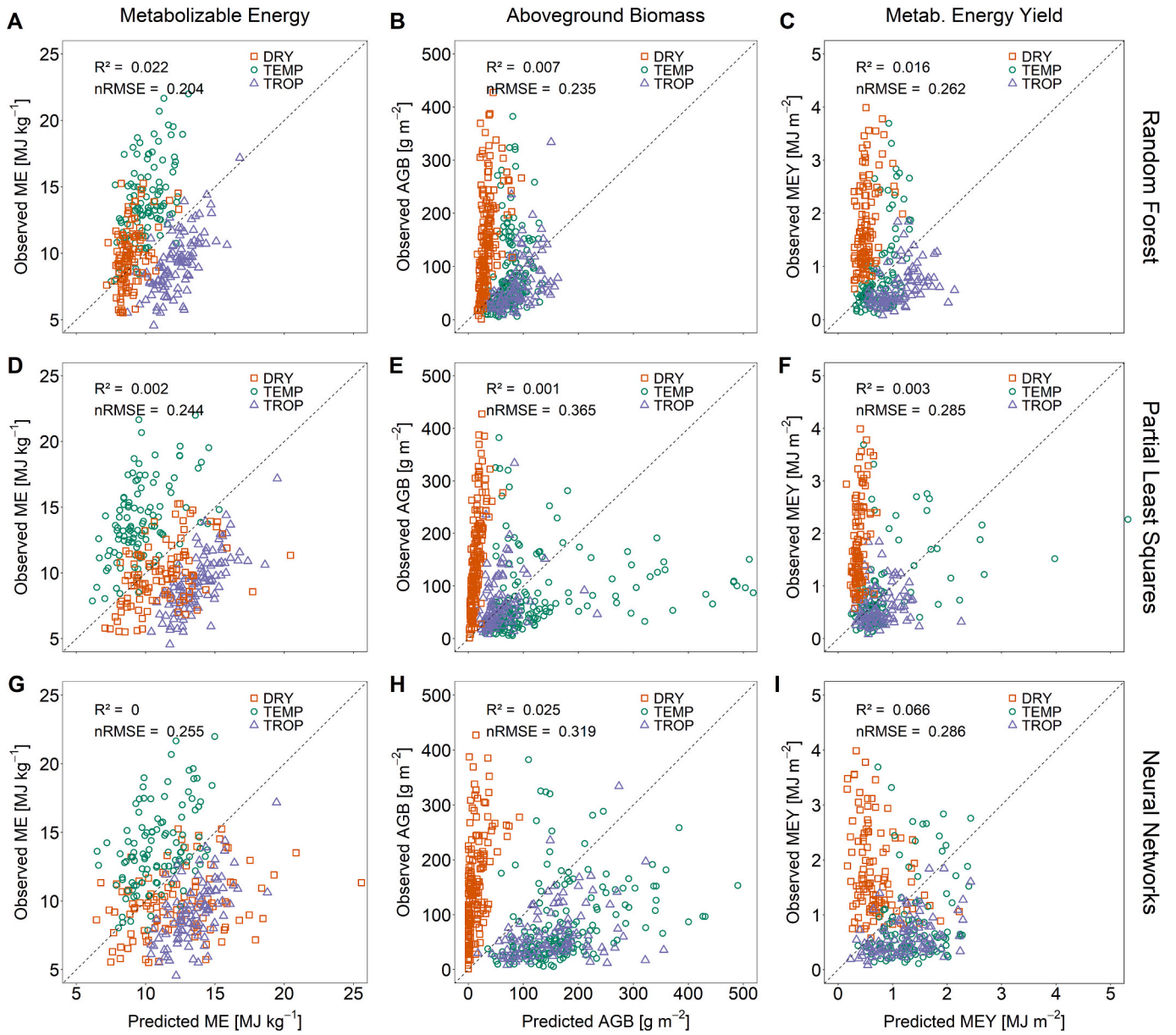

Fig. 8. Spatial cross-validation of prediction models for metabolizable energy (ME), aboveground biomass (AGB) and metabolizable energy yield (MEY) across three climatic regions. Model performance was evaluated using spatial cross-validation, where quality metrics were derived from the combined validation data of three transfer scenarios: "TROP" (models trained on dry subhumid and temperate data, validated on tropical data), "DRY" (trained on temperate and tropical data, validated against dry subhumid data), and "TEMP" (trained on dry subhumid and tropical data, validated on temperate data). Predictions were made using random forest regression (A-C), partial least squares regression (D—F), and a one-dimensional convolutional neural network regression (G-I).

similar data volumes. On the one hand, one-dimensional neural networks can capture the proximity properties in sequential data. We thus expected them to perform well with hyperspectral data. On the other hand, ensemble models have been shown to outperform neural networks with tabular data in benchmark datasets (Shwartz-Ziv and Armon, 2021). However, our one-dimensional neural network models were consistently outperformed by random forest and partial least squares regression across global (Fig. 5), regional (Fig. 6) and global-to-regional (Fig. 7) transfer experiments. This highlights the need for algorithm selection on a case-by-case basis, as stated in the "no free lunch" theorem (Wolpert and Macready, 1997).

Forage quantity predictions were particularly sensitive to variations in foliar pigments (Gitelson et al., 1996; Pinar and Curran, 1996) and canopy structure (Näsi et al., 2018; Oliveira et al., 2019; Oliveira et al., 2020), which limits prediction accuracy, especially in canopies with a high biomass density (Fig. 6). In contrast, low aboveground biomass estimates in tropical and dry subtropical regions were influenced by bare soil reflectance contamination (Fig. 2 A). Similar to the limitations of visual cover estimations in assessing plant biomass (Reddersen et al., 2014), the saturation effect remains an unavoidable constraint of spectral observations (Wachendorf et al., 2018). Especially in dense swards, as observed in temperate grasslands, additional canopy structural information, e.g., plant height, LiDAR scans or 3D canopy structure, may account for vertical density and thus enhance biomass predictions (Näsi et al., 2018; Oliveira et al., 2019). Contrary to aboveground biomass, metabolizable energy predictions consistently demonstrated high accuracy across all algorithms. This is likely due to the strong correlation between canopy reflectance in shortwave infrared wavelengths and biochemical plant properties linked to metabolizable energy, particularly fibre constituents and proteins (Menke and Steingass, 1988;

Thenkabail et al., 2000). These components are not only key indicators of forage quality but are also closely associated with leaf traits such as leaf nitrogen content and structural investment. As such, they reflect plant functional strategies along gradients of resource acquisition and conservation, as conceptualized in the Leaf Economics Spectrum (Wright et al., 2004). Because these functional relationships are stable across diverse climatic and ecological contexts (Díaz et al., 2016; Gross et al., 2024) the underlying spectral signals remain robust (Melesse et al., 2013; Menke and Steingass, 1988; Tirfessa and Tolera, 2020), supporting the universal applicability of metabolizable energy prediction models across different regions or biomes. However, there are limitations to the application of these models in areas characterized by very low vegetation cover, where the reflectance spectrum is predominantly influenced by bare soil. Consequently, the training dataset for this study was restricted to a minimum of 40 % vegetation cover, which in turn limits the applicability of metabolizable energy models to sparser grassland ecosystems. To address this limitation, spectral unmixing methods could be employed to remove the soil signal, leveraging the known spectral signatures of specific soil types (Asner and Heidebrecht, 2002). It is crucial to apply these methods cautiously, as they may introduce noise into the datasets. An alternative approach could involve utilizing separate models for areas with high and low soil coverage or incorporating soil cover as a predictor variable, particularly for partial least squares or random forest models. Our global accuracy measures also align with published models for the prediction of metabolizable energy ($0.50 < R^2 < 0.83$) that were created for specific regional applications (Biewer et al., 2009; Duranovich et al., 2020; Ferner et al., 2015), reinforcing the feasibility of its global spectral-based estimation. More generally, our results are also encouraging for predicting other vegetation characteristics from reflectance data with global models, particularly if these characteristics are based on universally detectable plant traits such as foliar nitrogen concentration (Dehghan-Shoar et al., 2024) or neutral and acid detergent fibre (Fernández-Habas et al., 2022). On the other hand, it shows limitations for global prediction of structural parameters like aboveground biomass.

Predictions of metabolizable energy consistently demonstrated intermediate levels of accuracy across all machine learning algorithms. This suggests that, when combined, the prediction accuracies of metabolizable energy and aboveground biomass tend to converge or offset each other. Our findings support our first hypothesis regarding the predictability of forage quality but do not support it for biomass or combined energy yield. Thus, structural differences among grasslands across global regions – such as variation in canopy architecture and vegetation density – pose significant challenges to universal spectral prediction of biomass-related proxies.

4.4. Global-to-regional transferability

Evaluating the transferability of a global model to a specific region provided valuable insights into the feasibility of global prediction models. Our results highlight that transferability was strongly influenced by the choice of algorithm, whereas the specific forage proxies and climatic regions had only minor effects. Comparing globally trained models to regionally trained counterparts revealed only minor accuracy differences, with regional models tendentially performing slightly better in most cases (Fig. 7 B). Algorithm choice also played a crucial role in transferability. Globally trained neural networks tended to outperform their regionally trained counterparts, whereas partial least squares models performed better when trained regionally. Our findings align with previous studies where neural networks were found to outperform partial least squares or cubist models at high sample numbers, while the superiority decreased at smaller sample sizes and local levels (Ng et al., 2022; Padarian et al., 2019b). On the contrary, some studies have shown higher performance of neural networks compared to partial least squares models even at lower sample numbers (Kawamura et al., 2021). This duality can be attributed to several theoretical factors. First, convolutive neural networks typically require large datasets and introduce more parameters than the other two algorithms. In smaller regional datasets, limited sample sizes may thus lead to underfitting or unstable optimization, reducing performance. (Meng et al., 2022; Padarian et al., 2019a). Partial least squares regression and random forest models, on the other hand, require region-specific training for optimal performance (Ng et al., 2022). The hierarchical feature learning of the neural networks, in combination with regularization through convolutional weights, may be able to extract latent spectral features that may be less sensitive to local domain shifts, improving transferability across regions. In our case, this manifested as lower local accuracy but higher robustness when applying globally trained neural networks to new regions—suggesting that these algorithms may be better suited for tasks requiring cross-domain generalization, despite their limitations in small-sample settings.

To our knowledge, this is the first study to directly compare different modelling algorithms in terms of their ability to transfer prediction models from global to regional scales. Our findings demonstrate that such comparisons can provide valuable guidance on whether site-specific or universal model are more appropriate for predicting forage-related variables. However, because no consistent trend emerged in favour of either global or regional models across all target variables and regions, our second hypothesis cannot be universally confirmed or rejected.

4.5. Between-region transferability

Global models exhibited limited transferability to regions excluded from the training process. Our study design, which encompasses diverse climatic and management gradients, successfully captured a broad spectrum of grassland vegetation. While this broad ecological representation provides a strong foundation for global models, it might hamper between-region transferability. Most importantly, the ecological variation in our dataset was reduced by one third in this test, as spatial cross-validation required the omission of one region for validation. To improve model transferability, training datasets for global models should ideally include more than three climate regions. As our spatial cross-validation demonstrated, capturing a broad ecological variation in grass species' functional strategies across regional datasets can improve the robustness of global models but can reduce regional transferability, supporting our second hypothesis. In our case, however, the reduction of our dataset and thus the ecological variation in our training dataset, various biases and effects have become more prominent.

First, the transferability of biomass and energy yield prediction models was particularly constrained in the dry subtropical region, where values were consistently underestimated. This likely reflects regional differences in vertical biomass distribution, plant density, and average plant height (Fig. 2). Canopy structure influences spectral signatures by altering the proportion of plant material exposed to the sensor's field of view, especially in tall (dry subhumid region) versus short vegetation (dry subtropical and temperate region). This effect may have been enforced by differences in measurement height across regions – 1.3 m in the humid tropics and 1.5 m in the temperate and dry subtropical regions. Lower sensor height increases the prominence of upper canopy layers, potentially introducing a systematic bias. Such measurement inconsistencies underscore the need for standardized field protocols across regions (Halbritter et al., 2020). Second, dominant photosynthetic pathways may have affected model transferability and generalizability. Reflectance signatures can vary significantly between C_3 and C_4 plants, including grasses (Cushnahan et al., 2024; Shoko et al., 2016). In our dataset, C_4 grasses dominated the humid tropical and dry subtropical sites (Ferner et al., 2018; Menestrey Schwieger et al., 2025), while C_3 grasses prevailed in temperate grasslands (Meyer et al., 2025), suggesting that species composition may further constrain cross-regional model transfer. Third, temporal differences in data collection may have introduced additional variability. Tropical grassland data

were collected in 2012, while the other two regions were sampled in 2020–2021. However, since the weather conditions are quite different between the three regions, even within the same year, the bias of the different years might be minor compared to the climatic variations. Although a white reference panel was used to calibrate field measurements, we recommend an annual lab-based recalibration to further minimize the annual effect, as the reflectance of the panels can change over time due to changes in the material properties or the measuring accuracy of the measuring devices. Fourth, soil reflectance contamination – particularly under sparse vegetation in the dry subtropical grassland (Fig. 2a) may have reduced model robustness. As the relationship between soil cover and biomass varies regionally, applying soil-adjusted or narrowband vegetation indices (e.g. OSAVI) could improve prediction (Amputu et al., 2023; Thenkabail et al., 2000; Vidican et al., 2023). More advanced solutions, such as spectral unmixing with locally acquired soil spectra, may further enhance model generalizability under heterogenous environmental conditions.

Using a geographically extensive dataset, our results demonstrated the potential of global forage prediction models. Although we developed robust machine learning models, especially for forage quality, we found no evidence of their spatial transferability to regions outside the training set. This limitation was particularly evident in the results from random forest and partial least squares models, which produced less variable and more consistent point clouds than neural network models. This pattern may stem from insufficient domain adaptation, a well-known challenge in machine learning models, to which random forest and partial least squares algorithms appear more susceptible (Meyer and Pebesma, 2021; Muro et al., 2022). Recent domain adaptation techniques offer promising solutions to the challenges of transferability across climate regions. For example, the SpectralEarth hyperspectral database based on EnMAP, with thousands of globally distributed data points, could be used to pretrain foundation models with improved generalization (Braham et al., 2025). Additionally, some studies suggest identifying domain-invariant features to reduce noise from local variations such as species composition, management, soil types, or atmospheric and illumination conditions (Xu et al., 2023). However, these features tend to be target-variable specific, and currently, no hyperspectral dataset exists with sufficient cross-continental coverage and standardized agronomic labelling to fully support such approaches in our context. This underscores the critical need for future data collection efforts that encompass ecological gradients and include consistent pasture quality measurements.

Although our prediction method is based on field spectroscopy data, it has the potential to replace conventional methods for assessing grassland traits (Fernández-Habas et al., 2022; Ferner et al., 2015). In the future, the prediction algorithms are meant to be adapted and upscaled to airborne or space-based multi- and hyperspectral image data from drone cameras and satellite push broom scanners (Ferner et al., 2021; Oliveira et al., 2024; Sahoo et al., 2024). The application of satellite-based hyperspectral data from current and future missions, such as EnMAP and the Copernicus Hyperspectral Imaging Mission for the Environment (CHIME), presents significant potential (Ghazaryan et al., 2024). However, several challenges must be addressed to successfully upscale these findings to hyperspectral imagery. Key hurdles include adapting field sampling protocols to align with the spatial resolution of the satellites, accounting for the spectral resolution of each band in upcoming missions, and addressing issues related to bare soil interference. Additionally, the robustness of models must be evaluated against region-specific seasonal vegetation dynamics that influence predictions of forage quality and quantity. If these challenges are overcome, the upscaling to drone or satellite imagery could facilitate the derivation of forage quality and biomass metrics for specific grassland areas using multi- and hyperspectral data. This information would be crucial for grassland managers in optimizing grazing strategies, including the timing and stocking density of livestock units. Beyond agricultural applications, these insights could enhance nature conservation and sustainable grassland management. They would support grassland health monitoring by focusing on vegetation properties, such as assessing vegetation condition through models estimating digestibility of aboveground biomass as an ecosystem function, measuring it as annual net primary productivity, and advancing models for taxonomic and functional diversity (Iakunin et al., 2025; Liu et al., 2021a; Muro et al., 2022; Pi et al., 2021; Schiefer et al., 2023). Regular spectral measurements obtained from spectrometers, drones, or satellite imagery could facilitate long-term monitoring of grassland health, serving as a valuable decision-making tool for conservation policies and climate change monitoring efforts.

5. Conclusions

We developed a novel spectral prediction approach to estimate forage quantity and quality proxies across global grassland biomes, based on a harmonized dataset capturing broad environmental variability. Using different machine learning algorithms within a three-step evaluation framework, we assessed global model performance and transferability both within and across regions. Our findings provide important insights into the potential and limitations of hyperspectral models for forage provision monitoring, highlighting the superior performance of random forest models and the consistent accuracy of forage quality predictions, likely due to strong correlations of spectral features with quality-related plant functional traits. Forage quantity was more challenging to predict due to region-specific variations in canopy structure and leaf pigment content. While our approach aimed to develop fully generalised models, transferability was only feasible when models remained flexible enough to account for local variability. The implementation of enhanced standardized protocols, alongside adapted processing and learning methodologies, may help address these variabilities and contribute to the development of more generalizable models in future research.

Expanding the exploration of global grasslands with hyperspectral remote sensing imagery from new satellite missions combined with improved data on forage quality and quantity, could increase model accuracy and predictive reliability beyond the current training datasets. Future models should also become more mechanistically oriented, focusing on causal relationships between grassland characteristics and reflectance rather than purely statistical associations. Beyond agricultural applications, spectroscopy-based models could significantly advance biodiversity conservation and sustainable grassland management. More accurate and scalable predictions of grassland properties would enable improved monitoring and understanding of biodiversity-ecosystem service relationships in agroecological landscapes, supporting more effective conservation strategies and sustainable land use worldwide.

Declaration of AI and AI-assisted technologies in the writing process

During the preparation of this work the authors used ChatGPT based on GPT-3.5/OpenAI and DeepL from DeepL SE Cologne to improve readability and language. After using this tool, the authors reviewed and edited the content as needed and take full responsibility for the content of the publication.

CRediT authorship contribution statement

Florian A. Männer: Writing – original draft, Visualization, Methodology, Investigation, Formal analysis, Data curation, Conceptualization. **Javier Muro:** Writing – review & editing, Investigation, Formal analysis, Conceptualization. **Olena Dubovyk:** Writing – review & editing, Project administration, Funding acquisition, Conceptualization. **Jessica Ferner:** Methodology, Investigation, Data curation. **Reginald Tang Guuroh:** Methodology, Investigation, Data curation. **Nichola M.**

Knox: Writing – review & editing, Methodology, Data curation. **Sebastian Schmidtlein:** Writing – review & editing, Project administration, Methodology, Funding acquisition. **Anja Linstädter:** Writing – review & editing, Supervision, Project administration, Methodology, Investigation, Funding acquisition, Conceptualization.

Funding sources

This work was funded by the DFG Priority Program 1374 within the framework of the SeBAS project (LI 1842/4-1 and DU 1596/1-1); by the German Federal Ministry of Research, Technology and Space (BMFTR) through the NamTip project within the BioTip and GlobalTip funding lines (FKZ 01LC1821A and 01LC2321A), and through the WASCAL initiative (01LG1202A). AL also acknowledges funding through the BMFTR-funded WASCAL WRAP 2.0 initiative (GreenGaDe project, grant 01LG2078A).

Declaration of competing interest

The authors declare that they have no known competing financial interests or personal relationships that could have appeared to influence the work reported in this paper.

Acknowledgements

The authors want to thank Karlheinz Südekum, Christian Böttger, Katharina Wild, and Nicolas C. Klein for their support with respect to the in-vitro gas production test of forage quality, and Mark C. Bilton, Uhangatenua Kapi, Lisa-Maricia Schwarz, Vistorina Amputu, and numerous student assistants for their help with the fieldwork. We also thank Zbyněk Malenovský for the support in processing and interpretation of the hyperspectral readings and his constructive feedback on an earlier draft of the manuscript. We thank the managers of three Biodiversity Exploratories (Germany), Max Müller, Julia Bass, Robert Künast, Miriam Teuscher, Anna K. Franke, Uta Schumacher, Franca Marian and all former managers for their work in maintaining the plot and project infrastructure; Victoria Grießmeier for giving support through the central office, Andreas Ostrowski for managing the central database, and Markus Fischer, Eduard Linsenmair, Dominik Hessenmöller, Daniel Prati, Ingo Schöning, François Buscot, Ernst-Detlef Schulze, Wolfgang W. Weisser and the late Elisabeth Kalko for their role in setting up the Biodiversity Exploratories project. We thank the administration of the Hainich national park, the UNESCO Biosphere Reserve Swabian Alb and the UNESCO Biosphere Reserve Schorfheide-Chorin for the excellent collaboration. Fieldwork permits for Germany were issued by the responsible state environmental offices of Baden-Württemberg, Thüringen, and Brandenburg. We acknowledge Stefan Liehr for his role in setting up the NamTip project, and Eike Kiene and Thomas Bringhenti for coordinating this project. Thanks to the Namibian National Commission on Research, Science and Technology we were allowed to conduct research and collect data in the Greater Waterberg Landscape (Permit Numbers: RPIV01162020, RPIV01042038). Many thanks to all farmers for granting us access to their rangelands, pastures and meadows.

Appendix A. Appendix

A.1. Figure of regional precipitation

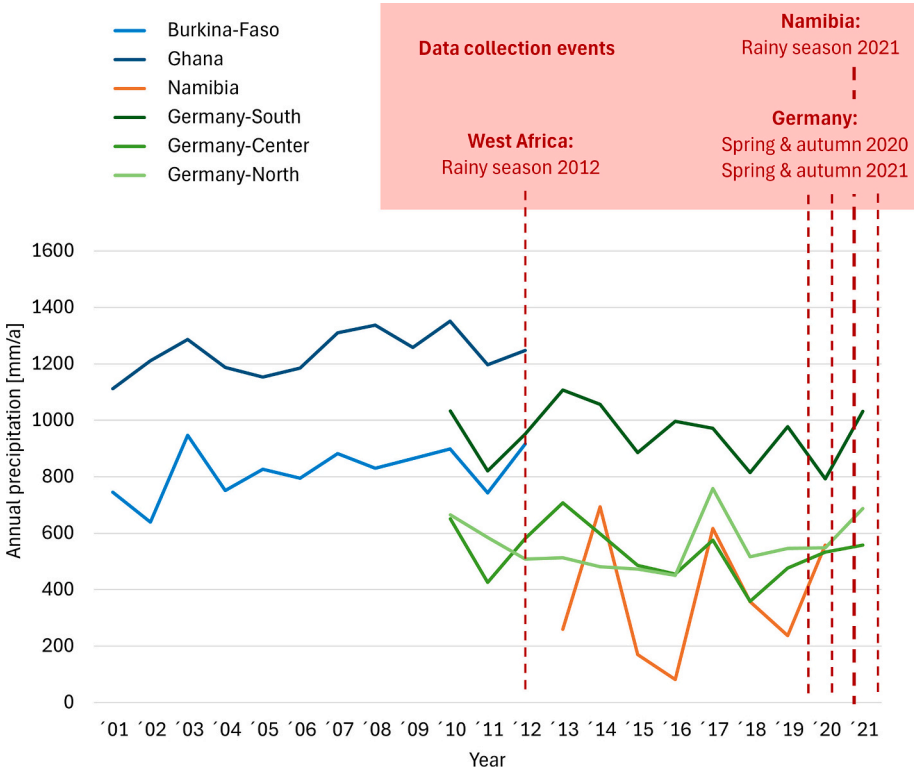

Fig. A1. Precipitation data from the 10 years before data collection for each site. Each line ends in the last year, the data were collected, except for Namibia, where data were collected in 2021, but no data were available for the last year. The data for Ghana and Burkina-Faso were downloaded from the Climate Change Knowledge Portal, where only country specific data were available (World Bank Group, 2021), the Namibian data were downloaded from the SASSCAL WeatherNet Dataset (SASSCAL WeatherNet, 2020) and the German data were collected from the BExIS dataset of the Biodiversity Exploratories (BExIS, 2019).

A.2. Table of all predictor tests

Table A1
Model qualities for metabolizable energy, biomass, and metabolizable energy yield using random forest (RF) and partial least squares (PLS) regression with different sets of input variables. Only relative reflectance, their first derivative, common vegetation indices and absorption characteristics, a combination of feature selection and first derivative, a combination of spectra and first derivative and the entire predictor set of spectra, first derivative and selected features were tested as input variable sets. The coefficient of determination (R^2), root mean square error (RMSE), and normalized RMSE (nRMSE) were calculated as quality parameters. For each scenario, hyperparameters such as the number of trees (ntree) for RF and the number of latent vectors (LV) used for PLS are reported along with the final number of predictors (Preds) chosen.

			Metabolizable Energy (ME)					Biomass (AGB)					Metabolizable Energy Yield (MEY)				
Algo-rithm	Spectral Input	Region	R^2	RMSE	nRMSE	ntree/ LV	Preds	R^2	RMSE	nRMSE	ntree/ LV	Preds	R^2	RMSE	nRMSE	ntree/ LV	Preds
RF	Reflectance spectra	Comb	0.464	1.233	0.133	400	53	0.312	2.008	0.122	400	34	0.225	1.991	0.177	50	168
		Trop	0.144	1.258	0.173	400	53	0.348	1.827	0.164	400	34	0.145	1.569	0.145	50	168
		Dry	0.422	1.195	0.175	400	53	0.563	1.653	0.088	400	34	0.253	1.463	0.197	50	168
		Temp	0.454	1.172	0.155	400	53	0.26	2.018	0.166	400	34	0.408	1.626	0.139	50	168
	First derivative of spectra	Comb	0.686	1.165	0.097	500	30	0.598	1.688	0.092	450	35	0.642	1.586	0.119	350	22
		Trop	0.466	1.177	0.123	500	30	0.512	1.591	0.126	450	35	0.38	1.506	0.131	350	22
		Dry	0.614	1.146	0.134	500	30	0.644	1.557	0.078	450	35	0.441	1.363	0.161	350	22
		Temp	0.548	1.17	0.153	500	30	0.525	1.797	0.138	450	35	0.584	1.72	0.155	350	22
	Feature selection	Comb	0.636	1.192	0.111	400	46	0.584	1.738	0.097	500	34	0.631	1.635	0.127	400	13
		Trop	0.442	1.178	0.123	400	46	0.459	1.602	0.128	500	34	0.278	1.64	0.159	400	13
		Dry	0.449	1.176	0.159	400	46	0.629	1.507	0.072	500	34	0.449	1.357	0.158	400	13
		Temp	0.575	1.149	0.135	400	46	0.561	1.715	0.128	500	34	0.606	1.699	0.152	400	13
	Feature selection & first derivative	Comb	0.693	1.169	0.099	300	27	0.617	1.71	0.094	400	58	0.664	1.588	0.119	500	32
		Trop	0.517	1.166	0.116	300	27	0.503	1.584	0.125	400	58	0.391	1.625	0.155	500	32
		Dry	0.613	1.182	0.165	300	27	0.659	1.476	0.068	400	58	0.445	1.374	0.165	500	32
		Temp	0.545	1.143	0.13	300	27	0.592	1.724	0.129	400	58	0.62	1.731	0.156	500	32
	Spectra & first derivative	Comb	0.685	1.177	0.103	450	16	0.598	1.791	0.102	450	49	0.639	1.609	0.123	200	49
		Trop	0.43	1.186	0.128	450	16	0.496	1.68	0.141	450	49	0.397	1.518	0.134	200	49
		Dry	0.602	1.148	0.135	450	16	0.666	1.489	0.07	450	49	0.456	1.352	0.156	200	49
		Temp	0.532	1.147	0.133	450	16	0.535	1.723	0.129	450	49	0.584	1.6	0.135	200	49
	All predictors (Spectra, first derivative and Feature selection)	Comb	0.691	1.175	0.102	450	23	0.617	1.734	0.096	250	50	0.661	1.603	0.121	450	58
		Trop	0.476	1.214	0.146	450	23	0.493	1.56	0.121	250	50	0.391	1.451	0.12	450	58
		Dry	0.597	1.147	0.135	450	23	0.647	1.556	0.077	250	50	0.464	1.405	0.176	450	58
		Temp	0.567	1.151	0.137	450	23	0.575	1.76	0.134	250	50	0.614	1.425	0.102	450	58
PLS	Reflectance spectra	Comb	0.624	1.198	0.115	9	87	0.528	1.829	0.106	11	135	0.155	2.076	0.188	3	97
		Trop	0.564	1.173	0.12	9	87	0.444	1.681	0.141	11	135	0.417	1.555	0.142	3	97
		Dry	0.612	1.159	0.145	9	87	0.614	1.634	0.086	11	135	0.412	1.404	0.176	3	97
		Temp	0.536	1.158	0.143	9	87	0.53	1.801	0.14	11	135	0.43	1.809	0.17	3	97
	First derivative of spectra	Comb	0.669	1.185	0.108	6	153	0.499	1.863	0.109	7	80	0.603	1.65	0.129	6	51
		Trop	0.601	1.165	0.115	6	153	0.452	1.675	0.14	7	80	0.344	1.597	0.151	6	51
		Dry	0.588	1.164	0.15	6	153	0.554	1.695	0.093	7	80	0.406	1.406	0.177	6	51
		Temp	0.456	1.172	0.155	6	153	0.412	1.931	0.156	7	80	0.446	1.794	0.168	6	51
	Feature selection	Comb	0.572	1.213	0.122	5	170	0.395	1.981	0.12	3	170	0.371	1.878	0.162	2	170
		Trop	0.192	1.243	0.164	5	170	0.381	1.73	0.149	3	170	0.309	1.617	0.155	2	170
		Dry	0.467	1.189	0.17	5	170	0.589	1.661	0.089	3	170	0.419	1.401	0.175	2	170
		Temp	0.598	1.147	0.133	5	170	0.371	1.975	0.161	3	170	0.485	1.757	0.162	2	170
	Feature selection & first derivative	Comb	0.651	1.19	0.111	6	323	0.424	1.948	0.117	4	261	0.562	1.692	0.135	4	323
		Trop	0.377	1.21	0.144	6	323	0.517	1.623	0.132	4	261	0.391	1.57	0.145	4	323
		Dry	0.591	1.163	0.148	6	323	0.602	1.647	0.087	4	261	0.457	1.385	0.169	4	323
		Temp	0.588	1.148	0.135	6	323	0.509	1.825	0.143	4	261	0.563	1.681	0.149	4	323
	Spectra & first derivative	Comb	0.664	1.186	0.109	11	109	0.494	1.868	0.11	10	136	0.609	1.643	0.128	9	136
		Trop	0.587	1.168	0.117	11	109	0.483	1.65	0.136	10	136	0.362	1.587	0.148	9	136
		Dry	0.581	1.166	0.151	11	109	0.599	1.65	0.088	10	136	0.488	1.372	0.164	9	136
		Temp	0.653	1.135	0.124	11	109	0.467	1.871	0.148	10	136	0.48	1.76	0.162	9	136
	All predictors (Spectra, first derivative and Feature selection)	Comb	0.689	1.179	0.105	9	491	0.45	1.919	0.114	5	491	0.59	1.663	0.131	6	491
		Trop	0.129	1.253	0.17	9	491	0.518	1.622	0.132	5	491	0.337	1.601	0.151	6	491
		Dry	0.614	1.159	0.145	9	491	0.617	1.632	0.086	5	491	0.424	1.399	0.174	6	491
		Temp	0.527	1.16	0.144	9	491	0.486	1.85	0.146	5	491	0.495	1.746	0.16	6	491

A.3. Predictor importance of all used predictors

Table A2
Relative predictor importances of the selected first derivatives per band. For each forage proxy, a different predictor set was selected for each of the machine learning algorithm. The importance measures were extracted from the training output and normalized, if required. Empty fields mean, the first derivative of the band was not used as predictor for the prediction model of the respective forage proxy. The results are also visualized in Fig. A2.

Band in nm	ME			AGB			MEY		
	RF	PLS	cNN	RF	PLS	cNN	RF	PLS	cNN
450	0.1226	0.0110	0.0108			0.0108			0.0108
460	0.0292	0.0070	0.0068	0.0286		0.0068	0.0348		0.0068
470		0.0053	0.0031			0.0031			0.0031
480		0.0057	0.0042			0.0042			0.0042
490	0.0164	0.0061	0.0088			0.0088			0.0088
500		0.0069	0.0072			0.0072			0.0072
510		0.0056	0.0028		0.0168	0.0028		0.0226	0.0028
520		0.0064	0.0049		0.0114	0.0049		0.0193	0.0049
530		0.0063	0.0203		0.0114	0.0203		0.0147	0.0203
540		0.0032	0.0061		0.0124	0.0061			0.0061
550	0.0212	0.0053	0.0108		0.0084	0.0108			0.0108
560		0.0055	0.0045		0.0042	0.0045		0.0213	0.0045
570		0.0059	0.0013		0.0053	0.0013		0.0207	0.0013
580		0.0064	0.0049		0.0039	0.0049		0.0213	0.0049
590		0.0059	0.0013		0.0055	0.0013		0.0248	0.0013
600		0.0052	0.0030		0.0043	0.0030		0.0215	0.0030
610		0.0056	0.0008		0.0106	0.0008		0.0217	0.0008
620		0.0054	0.0016		0.0134	0.0016			0.0016
630		0.0061	0.0096			0.0096			0.0096
640		0.0057	0.0013		0.0039	0.0013		0.0207	0.0013
650		0.0066	0.0035		0.0242	0.0035			0.0035
660		0.0071	0.0048		0.0227	0.0048		0.0186	0.0048
670	0.0239	0.0097	0.0046			0.0046			0.0046
680		0.0051	0.0178			0.0178			0.0178
690		0.0056	0.0039		0.0114	0.0039		0.0183	0.0039
700		0.0055	0.0022		0.0081	0.0022		0.0138	0.0022
710		0.0054	0.0007		0.0095	0.0007		0.0110	0.0007
720		0.0057	0.0022		0.0096	0.0022		0.0094	0.0022
730		0.0066	0.0032		0.0079	0.0032		0.0062	0.0032
740		0.0079	0.0030		0.0087	0.0030		0.0114	0.0030
750	0.0183	0.0091	0.0015		0.0089	0.0015		0.0160	0.0015
760	0.0229	0.0135	0.0056		0.0092	0.0056		0.0266	0.0056
770		0.0050	0.0021	0.0237	0.0110	0.0021			0.0021
780	0.0171	0.0068	0.0034			0.0034			0.0034
790		0.0066	0.0028			0.0028			0.0028
800		0.0066	0.0047			0.0047			0.0047
810		0.0082	0.0030	0.0211	0.0129	0.0030		0.0134	0.0030
820	0.0332	0.0072	0.0058			0.0058	0.0288		0.0058
830		0.0042	0.0056	0.0232		0.0056	0.0263		0.0056
840	0.0212	0.0058	0.0070	0.0153		0.0070			0.0070
850		0.0063	0.0067			0.0067			0.0067
860		0.0042	0.0087			0.0087			0.0087
870		0.0053	0.0079			0.0079			0.0079
880		0.0058	0.0104			0.0104			0.0104
890		0.0063	0.0076		0.0145	0.0076		0.0096	0.0076
900		0.0031	0.0014		0.0184	0.0014		0.0206	0.0014
910		0.0068	0.0042		0.0079	0.0042		0.0122	0.0042
920		0.0030	0.0041		0.0127	0.0041		0.0182	0.0041
930		0.0086	0.0102		0.0074	0.0102		0.0152	0.0102
940		0.0040	0.0038		0.0190	0.0038		0.0180	0.0038
950		0.0050	0.0031	0.0165	0.0159	0.0031		0.0257	0.0031
960	0.0131	0.0138	0.0075		0.0163	0.0075	0.0499	0.0422	0.0075
970		0.0043	0.0053		0.0111	0.0053			0.0053
980		0.0089	0.0054		0.0100	0.0054			0.0054
990		0.0057	0.0106			0.0106			0.0106
1000		0.0039	0.0094			0.0094			0.0094
1010		0.0043	0.0147		0.0119	0.0147			0.0147
1020		0.0043	0.0009		0.0123	0.0009			0.0009
1030		0.0045	0.0053		0.0092	0.0053			0.0053
1040		0.0059	0.0042	0.0237		0.0042			0.0042
1050	0.0182	0.0059	0.0078	0.0282		0.0078	0.0404		0.0078
1060		0.0062	0.0151	0.0246		0.0151	0.0693		0.0151
1070		0.0048	0.0055			0.0055			0.0055
1080		0.0049	0.0028			0.0028			0.0028
1090		0.0049	0.0044	0.0185	0.0069	0.0044			0.0044
1100		0.0057	0.0015	0.0208	0.0086	0.0015	0.0291	0.0063	0.0015
1110		0.0058	0.0065	0.0190	0.0062	0.0065		0.0068	0.0065
1120		0.0051	0.0040	0.0317	0.0050	0.0040	0.0265	0.0126	0.0040

1130		0.0067	0.0076	0.0189	0.0119	0.0076		0.0148	0.0076
1140		0.0053	0.0015		0.0059	0.0015		0.0175	0.0015
1150		0.0077	0.0147	0.0809	0.0518	0.0147	0.1148	0.0663	0.0147
1160		0.0082	0.0047		0.0101	0.0047		0.0174	0.0047
1170	0.0166	0.0093	0.0044		0.0138	0.0044	0.0327		0.0044
1180		0.0099	0.0083	0.0321		0.0083	0.0461		0.0083
1190		0.0067	0.0059	0.0175		0.0059			0.0059
1200		0.0055	0.0053	0.0172		0.0053			0.0053
1210		0.0037	0.0205			0.0205			0.0205
1220		0.0033	0.0044			0.0044			0.0044
1230		0.0038	0.0091	0.0263		0.0091			0.0091
1240		0.0035	0.0103	0.0498		0.0103			0.0103
1250		0.0042	0.0086	0.0347		0.0086	0.0413		0.0086
1260		0.0052	0.0098			0.0098			0.0098
1270	0.0140	0.0047	0.0161			0.0161	0.0295		0.0161
1280		0.0049	0.0055		0.0144	0.0055		0.0180	0.0055
1290		0.0050	0.0004		0.0065	0.0004		0.0122	0.0004
1300		0.0052	0.0010		0.0043	0.0010		0.0089	0.0010
1310		0.0052	0.0006		0.0097	0.0006		0.0086	0.0006
1320		0.0054	0.0028		0.0120	0.0028		0.0101	0.0028
1330		0.0057	0.0092		0.0442	0.0092		0.0451	0.0092
1340		0.0055	0.0009		0.0240	0.0009		0.0159	0.0009
1500		0.0078	0.0073			0.0073			0.0073
1510		0.0080	0.0071			0.0071			0.0071
1520		0.0082	0.0019		0.0118	0.0019			0.0019
1530	0.0144	0.0084	0.0016		0.0104	0.0016			0.0016
1540		0.0085	0.0023		0.0089	0.0023			0.0023
1550	0.0169	0.0087	0.0034		0.0093	0.0034			0.0034
1560	0.0178	0.0088	0.0068		0.0101	0.0068			0.0068
1570	0.0196	0.0091	0.0086		0.0136	0.0086			0.0086
1580	0.0185	0.0086	0.0014			0.0014			0.0014
1590		0.0089	0.0036			0.0036			0.0036
1600		0.0091	0.0019			0.0019			0.0019
1610		0.0091	0.0082			0.0082			0.0082
1620		0.0082	0.0054			0.0054			0.0054
1630		0.0083	0.0108	0.0244		0.0108			0.0108
1640	0.0347	0.0107	0.0110	0.0287		0.0110	0.0267		0.0110
1650	0.1468	0.0116	0.0115	0.0539		0.0115	0.0349		0.0115
1660	0.1690	0.0135	0.0121	0.0342		0.0121	0.0422		0.0121
1670		0.0058	0.0037			0.0037			0.0037
1680	0.0160	0.0072	0.0267			0.0267			0.0267
1690	0.0241	0.0102	0.0072	0.0201		0.0072			0.0072
1700		0.0062	0.0089	0.0196		0.0089			0.0089
1710	0.0155	0.0063	0.0051			0.0051			0.0051
1720		0.0055	0.0115			0.0115			0.0115
1730		0.0053	0.0039	0.0414	0.0284	0.0039	0.0607		0.0039
1740		0.0072	0.0094	0.0186	0.0166	0.0094		0.0263	0.0094
1750		0.0059	0.0041		0.0184	0.0041			0.0041
1760		0.0072	0.0038			0.0038			0.0038
1770		0.0069	0.0126			0.0126			0.0126
1780		0.0068	0.0027			0.0027			0.0027
1790		0.0051	0.0045			0.0045			0.0045
2000		0.0057	0.0078			0.0078			0.0078
2010		0.0088	0.0142	0.0999	0.0321	0.0142	0.1081	0.0510	0.0142
2020		0.0071	0.0088		0.0283	0.0088			0.0088
2030		0.0046	0.0049			0.0049			0.0049
2040		0.0051	0.0076		0.0135	0.0076			0.0076
2050		0.0061	0.0106		0.0140	0.0106		0.0226	0.0106
2060		0.0079	0.0049	0.0251	0.0144	0.0049		0.0241	0.0049
2070		0.0093	0.0049		0.0141	0.0049			0.0049
2080	0.0171	0.0098	0.0045			0.0045			0.0045
2090		0.0091	0.0056			0.0056			0.0056
2100	0.0161	0.0135	0.0172			0.0172			0.0172
2110		0.0112	0.0083			0.0083			0.0083
2120		0.0074	0.0086			0.0086			0.0086
2130		0.0066	0.0084			0.0084			0.0084
2140		0.0062	0.0062			0.0062			0.0062
2150		0.0079	0.0175		0.0095	0.0175			0.0175
2160	0.0223	0.0076	0.0060		0.0070	0.0060			0.0060
2170	0.0165	0.0067	0.0072		0.0101	0.0072			0.0072

2180		0.0061	0.0139			0.0139			0.0139
2190		0.0044	0.0079			0.0079			0.0079
2200		0.0053	0.0068	0.0446	0.0086	0.0068	0.0602	0.0348	0.0068
2210		0.0063	0.0069	0.0171	0.0058	0.0069	0.0394		0.0069
2220		0.0058	0.0035		0.0064	0.0035	0.0585	0.0336	0.0035
2230		0.0072	0.0066			0.0066			0.0066
2240		0.0049	0.0069		0.0248	0.0069		0.0188	0.0069
2250		0.0042	0.0070		0.0143	0.0070		0.0136	0.0070
2260		0.0050	0.0052		0.0121	0.0052			0.0052
2270		0.0049	0.0142			0.0142			0.0142
2280	0.0467	0.0118	0.0095			0.0095			0.0095
2290		0.0085	0.0106			0.0106			0.0106
2300		0.0032	0.0074			0.0074			0.0074

A.4. Predictor selection for all forage proxies

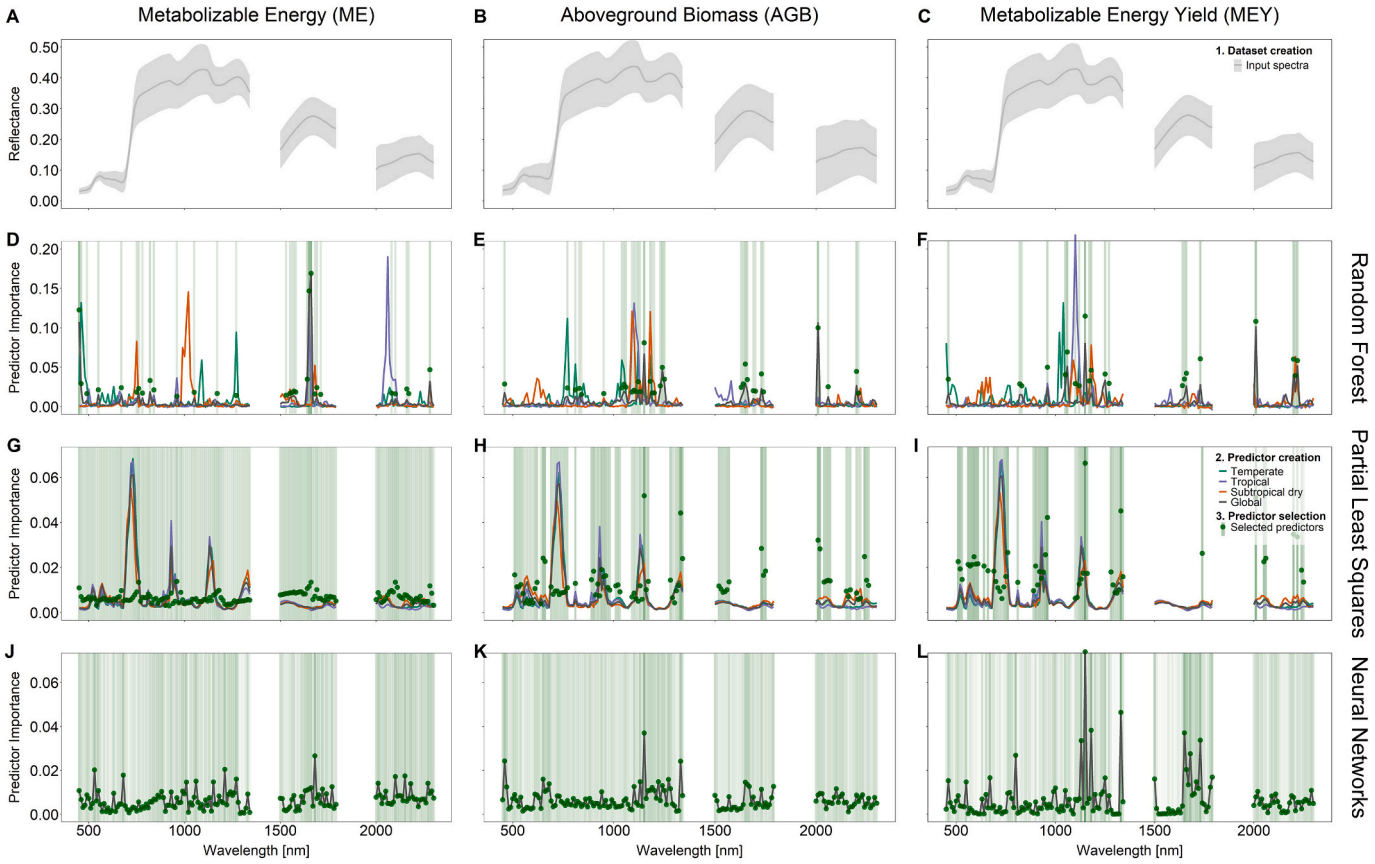

Fig. A2. Importance of single wavelengths (WL) from 450 nm to 2350 nm, using the first derivative of the canopy reflectance spectra, for predicting metabolizable energy (ME), aboveground biomass (AGB) and metabolizable energy yield (MEY) across RF regression, PLS regression, and a one-dimensional convolutional neural network. The grey line with the light grey shaded area represents the mean and standard deviation of the pure spectra input across all regions. Coloured lines indicate the importance of predictors for regional models, while black lines represent the global models. The green dots mark the final selected predictors for the prediction models and the green shading represent their relative importance in greenness intensity meaning higher importance. The white labels in the bottom graph name the spectral areas, where specific structures absorb in. The pigment area (Chlorophyll and Carotenoids) is located in the shorter wavelength area until 700 nm, the AGB area is represented between 700 and 1350 nm, while proteins absorb from 1500 nm upwards and fibre from 2000 nm in the measured spectrum. (For interpretation of the references to colour in this figure legend, the reader is referred to the web version of this article.)

A.5. Figure of 5-fold CV of all forage proxies, regions and algorithms

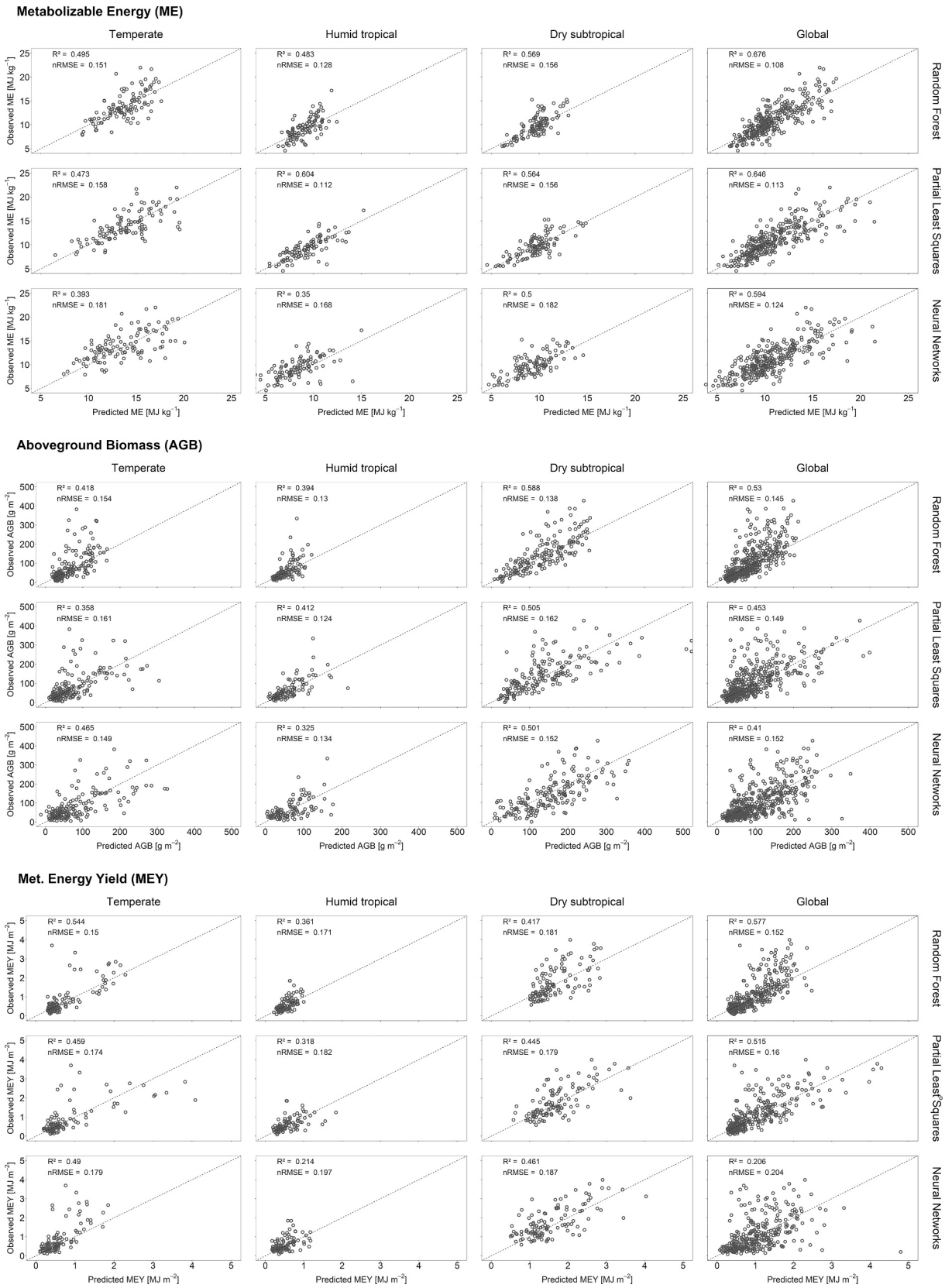

Fig. A3. 5-fold cross validation results for the regional and global prediction models for metabolizable energy (ME - top), biomass (AGB - middle) and metabolizable energy yield (MEY - bottom) using random forest regression, partial least squares regression and a 1-dimensional convolutional neural network.

A.6. Figure of global-to-regional transfer of all algorithms across forage proxies

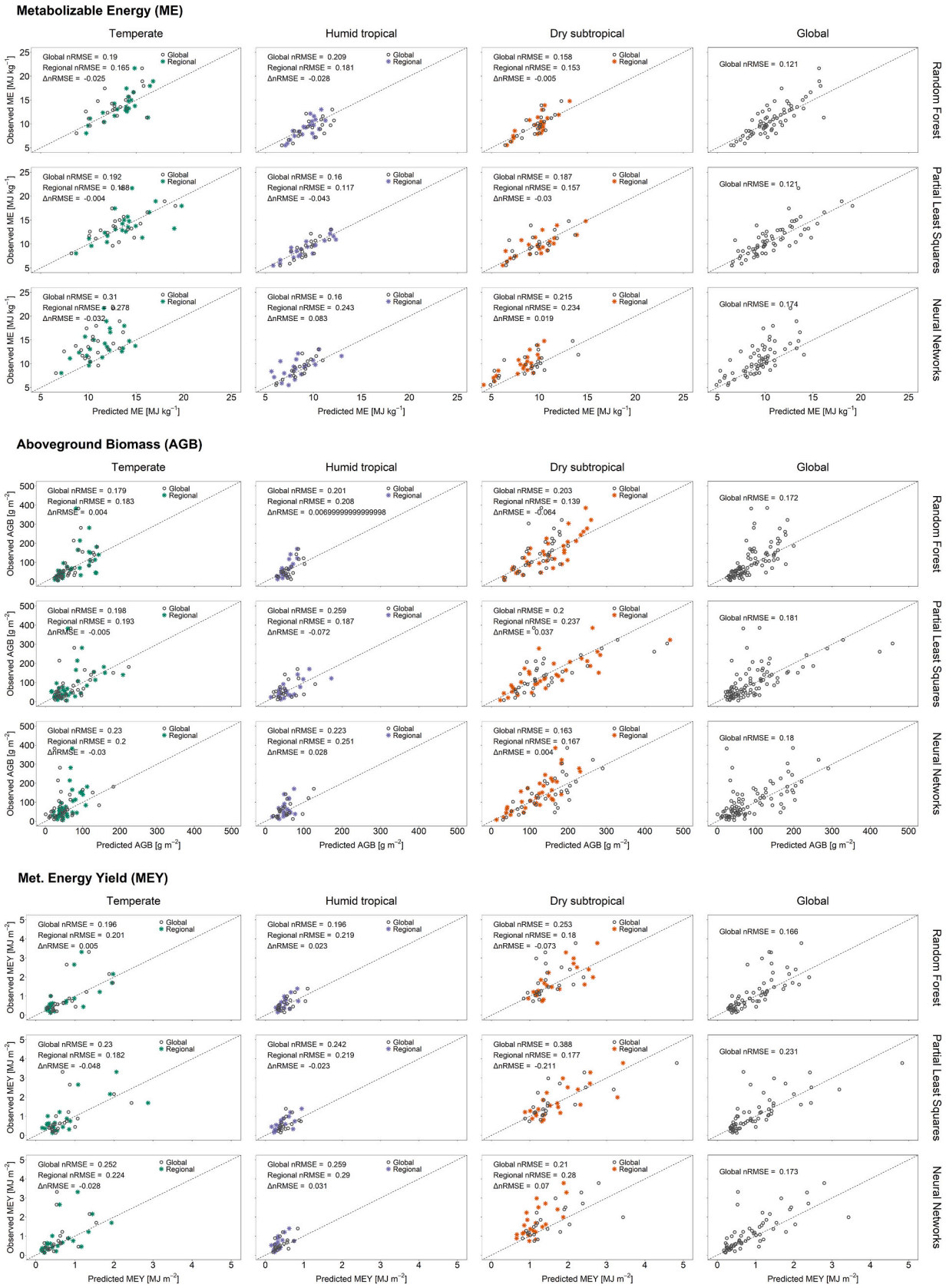

Fig. A4. Validation of the global ME, AGB and MEY prediction model in comparison with the respective regional prediction models using 20 % of the regional training data which were excluded from the training of both models. The black circles show the observed versus predicted data using the global model and the grey stars using the regional model respectively. The quality parameters are shown in the top left and bottom right corners. The trans-climatic column shows the results for

the global model only where 20 % of validation data from the tree regions were predicted by the model trained with the combined 80 % training data across the three regions.

Appendix B. Supplementary data

Supplementary data to this article can be found online at https://doi.org/10.1016/j.ecoinf.2025.103426.

Data availability

This work is partly based on data elaborated by the SeBAS project of the Biodiversity Exploratories program (DFG Priority Program 1374). The datasets from the German sites are publicly available in the Biodiversity Exploratories Information System BExIS (Männer, 2022).

The full spectral and laboratory data, including the data from BExIS and the used codes were published in the Mendeley Data Repository (Männer et al., 2025).

References

Amputu, V., Knox, N., Braun, A., Heshmati, S., Retzlaff, R., Röder, A., Tielbörger, K., 2023. Unmanned aerial systems accurately map rangeland condition indicators in a dryland savannah. Eco. Inform. 75, 102007. https://doi.org/10.1016/j.ecoinf.2023.102007.

Amputu, V., Männer, F.A., Tielbörger, K., Knox, N., 2024. Spatio-temporal transferability of drone-based models to predict forage supply in drier rangelands. Remote Sens 16, 1842. https://doi.org/10.3390/rs16111842.

Asner, G.P., Heidebrecht, K.B., 2002. Spectral unmixing of vegetation, soil and dry carbon cover in arid regions: comparing multispectral and hyperspectral observations. Int. J. Remote Sens. 23, 3939–3958. https://doi.org/10.1080/01431160110115960.

Atlas of Namibia Team, 2022. Atlas of Namibia: Its Land, Water and Life. Namibia Nature Foundation, Windhoek.

Bazzo, C.O.G., Kamali, B., Hütt, C., Bareth, G., Gaiser, T., 2023. A review of estimation methods for aboveground biomass in grasslands using UAV. Remote Sens 15, 639. https://doi.org/10.3390/rs15030639.

Bengtsson, J., Bullock, J.M., Egoh, B., Everson, C., Everson, T., O'Connor, T., O'Farrell, P. J., Smith, H.G., Lindborg, R., 2019. Grasslands — more important for ecosystem services than you might think. Ecosphere 10, e02582. https://doi.org/10.1002/ecs2.2582.

Bera, S., Shrivastava V., K., Chandra Satapathy, S., 2022. Advances in hyperspectral image classification based on convolutional neural networks: a review. Comput. Model. Eng. Sci. 133, 219–250. https://doi.org/10.32604/cmes.2022.020601.

BExIS, 2019. Open climate data of the Exploratories project: BExIS dataset ID 24766. In: Biodiversity Exploratories. https://www.bexis.uni-jena.de/tcd/PublicClimateData/Index (accessed 18 January 2025).

Biewer, S., Fricke, T., Wachendorf, M., 2009. Development of canopy reflectance models to predict forage quality of legume-grass mixtures. Crop Sci. 49, 1917–1926. https://doi.org/10.2135/cropsci2008.11.0653.

Blaix, C., Chabrerie, O., Alard, D., Catterou, M., Diquelou, S., Dutoit, T., Lacoux, J., Loucougaray, G., Michelot-Antalik, A., Pacé, M., Tardif, A., Lemauviel-Lavenant, S., Bonis, A., 2023. Forage nutritive value shows synergies with plant diversity in a wide range of semi-natural grassland habitats. Agric. Ecosyst. Environ. 347, 108369. https://doi.org/10.1016/j.agee.2023.108369.

Blüthgen, N., Dormann, C.F., Prati, D., Klaus, V.H., Kleinebecker, T., Hölzel, N., Alt, F., Boch, S., Gockel, S., Hemp, A., Müller, J., Nieschulze, J., Renner, S.C., Schöning, I., Schumacher, U., Socher, S.A., Wells, K., Birkhofer, K., Buscot, F., Oelmann, Y., Rothenwöhrer, C., Scherber, C., Tscharntke, T., Weiner, C.N., Fischer, M., Kalko, E.K. V., Linsenmair, K.E., Schulze, E.-D., Weisser, W.W., 2012. A quantitative index of land-use intensity in grasslands: integrating mowing, grazing and fertilization. Basic Appl. Ecol. 13, 207–220. https://doi.org/10.1016/j.baae.2012.04.001.

Boffa, J.-M., 1999. Agroforestry Parklands in Sub-Saharan Africa. Food and Agriculture Organization of the United Nations, Rome, 230 pp.

Braham, N.A.A., Albrecht, C.M., Mairal, J., Chanussot, J., Wang, Y., Zhu, X.X., 2025. SpectralEarth: training hyperspectral foundation models at scale. IEEE J. Sel. Top. Appl. Earth Observ. Remote Sens. 18, 16780–16797. https://doi.org/10.1109/JSTARS.2025.3581451.

Brinkmann, K., Schwieger, D.M., Grieger, L., Heshmati, S., Rauchecker, M., 2023. How and why do rangeland changes and their underlying drivers differ across Namibia's two major land tenure systems? Rangel. J. 5 (3), 123–139.

Callo-Concha, D., Gaiser, T., Webber, H., Tischbein, B., Ewert, F., 2013. Farming in the west African Sudan savanna: insights in the context of climate change. Afr. J. Agric. Res. 8, 4693–4705.

Chen, J.M., Rich, P.M., Gower, S.T., Norman, J.M., Plummer, S., 1997. Leaf area index of boreal forests: theory, techniques, and measurements. J. Geophys. Res. 102, 29429–29443. https://doi.org/10.1029/97JD01107.

Cook, R.D., Forzani, L., 2021. PLS regression algorithms in the presence of nonlinearity. Chemom. Intell. Lab. Syst. 213, 104307. https://doi.org/10.1016/j.chemolab.2021.104307.

Cunliffe, A.M., Brazier, R.E., Anderson, K., 2016. Ultra-fine grain landscape-scale quantification of dryland vegetation structure with drone-acquired structure-from-motion photogrammetry. Remote Sens. Environ. 183, 129–143. https://doi.org/10.1016/j.rse.2016.05.019.

Curran, P.J., 1989. Remote sensing of foliar chemistry. Remote Sens. Environ. 30, 271–278. https://doi.org/10.1016/0034-4257(89)90069-2.

Cushnahan, T.A., Grafton, M.C.E., Pearson, D., Ramilan, T., 2024. Hyperspectral data can differentiate species and cultivars of C3 and C4 turf despite measurable diurnal variation. Remote Sens 16. https://doi.org/10.3390/rs16173142.

Da Silveira Pontes, L., Maire, V., Schellberg, J., Louault, F., 2015. Grass strategies and grassland community responses to environmental drivers: a review. Agron. Sustain. Dev. 35, 1297–1318. https://doi.org/10.1007/s13593-015-0314-1.

Dehghan-Shoar, M.H., Kereszturi, G., Pullanagari, R.R., Orsi, A.A., Yule, I.J., Hanly, J., 2024. A physically informed multi-scale deep neural network for estimating foliar nitrogen concentration in vegetation. Int. J. Appl. Earth Obs. Geoinf. 130, 103917. https://doi.org/10.1016/j.jag.2024.103917.

Delegido, J., Verrelst, J., Alonso, L., Moreno, J., 2011. Evaluation of Sentinel-2 red-edge bands for empirical estimation of green LAI and chlorophyll content. Sensors (Basel, Switzerland) 11, 7063–7081. https://doi.org/10.3390/s110707063.

Díaz, S., Lavorel, S., McIntyre, S., Falczuk, V., Casanoves, F., Milchunas, D.G., Skarpe, C., Rusch, G., Sternberg, M., Noy-Meir, I., Landsberg, J., Zhang, L., Clark, A., Campbell, B.M., 2007. Plant trait responses to grazing - a global synthesis. Glob. Chang. Biol. 13, 313–341. https://doi.org/10.1111/j.1365-2486.2006.01288.x.

Díaz, S., Kattge, J., Cornelissen, J.H.C., Wright, I.J., Lavorel, S., Dray, S., Reu, B., Kleyer, M., Wirth, C., Colin Prentice, I., Garnier, E., Bönisch, G., Westoby, M., Poorter, H., Reich, P.B., Moles, A.T., Dickie, J., Gillison, A.N., Zanne, A.E., Chave, J., Joseph Wright, S., Sheremet'ev, S.N., Jactel, H., Baraloto, C., Cerabolini, B., Pierce, S., Shipley, B., Kirkup, D., Casanoves, F., Joswig, J.S., Günther, A., Falczuk, V., Rüger, N., Mahecha, M.D., Gorné, L.D., 2016. The global spectrum of plant form and function. Nature 529, 167–171. https://doi.org/10.1038/nature16489.

Dieste, Á.G., Argüello, F., Heras, D.B., Magdon, P., Linstädter, A., Dubovyk, O., Muro, J., 2024. ResNeTS: a ResNet for time series analysis of Sentinel-2 data applied to grassland plant-biodiversity prediction. IEEE J. Sel. Top. Appl. Earth Observ. Remote Sens. 17, 17349–17370. https://doi.org/10.1109/JSTARS.2024.3454271.

Duranovich, F.N., Yule, I.J., Lopez-Villalobos, N., Shadbolt, N.M., Draganova, I., Morris, S.T., 2020. Using proximal hyperspectral sensing to predict herbage nutritive value for dairy farming. Agronomy 10, 1826. https://doi.org/10.3390/agronomy10111826.

Evans, J.S., Murphy, M.A., Holden, Z.A., Cushman, S.A., 2011. Modeling species distribution and change using random forest. In: Drew, C.A., Wiersma, Y.F., Huettmann, F. (Eds.), PREDICTIVE Species and Habitat Modeling in Landscape Ecology: Concepts and Applications. Springer Science & Business Media, New York, Dordrecht, Heidelberg [etc.], pp. 139–159.

FAO, 1989. Soil Map of the World. Wageningen, pp. 1–138.

Féret, J.-B., Berger, K., de, Boissieu, F., Malenovský, Z., 2021. PROSPECT-PRO for estimating content of nitrogen-containing leaf proteins and other carbon-based constituents. Remote Sens. Environ. 252, 112173. https://doi.org/10.1016/j.rse.2020.112173.

Fernández-Habas, J., Carriere Cañada, M., García Moreno, A.M., Leal-Murillo, J.R., González-Dugo, M.P., Abellanas Oar, B., Gómez-Giráldez, P.J., Fernández-Rebollo, P., 2022. Estimating pasture quality of Mediterranean grasslands using hyperspectral narrow bands from field spectroscopy by random Forest and PLS regressions. Comput. Electron. Agric. 192, 106614. https://doi.org/10.1016/j.compag.2021.106614.

Ferner, J., Linstädter, A., Südekum, K.-H., Schmidtlein, S., 2015. Spectral indicators of forage quality in West Africa's tropical savannas. Int. J. Appl. Earth Obs. Geoinf. 41, 99–106. https://doi.org/10.1016/j.jag.2015.04.019.

Ferner, J., Schmidtlein, S., Guuroh, R.T., Lopatin, J., Linstädter, A., 2018. Disentangling effects of climate and land-use change on west African drylands' forage supply. Glob. Environ. Chang. 53, 24–38. https://doi.org/10.1016/j.gloenvcha.2018.08.007.

Ferner, J., Linstädter, A., Rogass, C., Südekum, K.-H., Schmidtlein, S., 2021. Towards forage resource monitoring in subtropical savanna grasslands: going multispectral or hyperspectral? Eur. J. Remote Sens. 54, 364–384. https://doi.org/10.1080/22797254.2021.1934556.

Fick, S.E., Hijmans, R.J., 2017. WorldClim 2: new 1-km spatial resolution climate surfaces for global land areas. Int. J. Climatol. 37, 4302–4315. https://doi.org/10.1002/joc.5086.

Finch, H., Samuel, A.M., Lane, G., 2002. 19 - Grazing. In: Finch, H., Samuel, A.M., Lane, G. (Eds.), Lockhart and Wiseman's Crop Husbandry Including Grassland (Eighth Edition) : Woodhead Publishing Series in Food Science, Technology and Nutrition. Woodhead Publishing, pp. 435–447.

Fischer, M., Bossdorf, O., Gockel, S., Hänsel, F., Hemp, A., Hessenmöller, D., Korte, G., Nieschulze, J., Pfeiffer, S., Prati, D., Renner, S., Schöning, I., Schumacher, U., Wells, K., Buscot, F., Kalko, E.K., Linsenmair, K.E., Schulze, E.-D., Weisser, W.W.,

2010. Implementing large-scale and long-term functional biodiversity research: the biodiversity Exploratories. Basic Appl. Ecol. 11, 473–485. https://doi.org/10.1016/j.baae.2010.07.009.
Garnier, E., Navas, M.-L., Grigulis, K., 2015. Plant Functional Diversity: Organism Traits, Community Structure, and Ecosystem Properties. Oxford University Press.
Getachew, G., Blümmel, M., Makkar, H., Becker, K., 1998. In vitro gas measuring techniques for assessment of nutritional quality of feeds: a review. Anim. Feed Sci. Technol. 72, 261–281. https://doi.org/10.1016/S0377-8401(97)00189-2.
Ghazaryan, G., Krupp, L., Seyfried, S., Landgraf, N., Nendel, C., 2024. Enhancing peatland monitoring through multisource remote sensing: optical and radar data applications. Int. J. Remote Sens. 45, 6372–6394. https://doi.org/10.1080/01431161.2024.2387133#d1e883.
Gibson, D.J., 2009. Grasses and Grassland Ecology. Oxford University Press, New York.
Giess, W., 1998. A Preliminary Vegetation Map of Namibia, 3rd ed. Namibia Scientific Society.
Gitelson, A.A., Merzlyak, M.N., Lichtenthaler, H.K., 1996. Detection of red edge position and chlorophyll content by reflectance measurements near 700 nm. J. Plant Physiol. 148, 501–508. https://doi.org/10.1016/S0176-1617(96)80285-9.
Gross, N., Maestre, F.T., Liancourt, P., Berdugo, M., Martin, R., Gozalo, B., Ochoa, V., Delgado-Baquerizo, M., Maire, V., Saiz, H., Soliveres, S., Valencia, E., Eldridge, D.J., Guirado, E., Jabot, F., Asensio, S., Gaitán, J.J., García-Gómez, M., Martínez, P., Martínez-Valderrama, J., Mendoza, B.J., Moreno-Jiménez, E., Pescador, D.S., Plaza, C., Pijuan, I.S., Abedi, M., Ahumada, R.J., Amghar, F., Arroyo, A.I., Bahalkeh, K., Bailey, L., Ben Salem, F., Blaum, N., Boldgiv, B., Bowker, M.A., Branquinho, C., van den Brink, L., Bu, C., Canessa, R., Del Castillo-Monroy, A.P., Castro, H., Castro, P., Chibani, R., Conceição, A.A., Darrouzet-Nardi, A., Davila, Y.C., Deák, B., Donoso, D.A., Durán, J., Espinosa, C., Fajardo, A., Farzam, M., Ferrante, D., Franzese, J., Fraser, L., Gonzalez, S., Gusman-Montalvan, E., Hernández-Hernández, R.M., Hölzel, N., Huber-Sannwald, E., Jadan, O., Jeltsch, F., Jentsch, A., Ju, M., Kaseke, K.F., Kindermann, L., Le Roux, P., Linstädter, A., Louw, M.A., Mabaso, M., Maggs-Kölling, G., Makhalanyane, T.P., Issa, O.M., Manzaneda, A.J., Marais, E., Margerie, P., Hughes, F.M., Messeder, J.V.S., Mora, J.P., Moreno, G., Munson, S.M., Nunes, A., Oliva, G., Oñatibia, G.R., Peter, G., Pueyo, Y., Quiroga, R. E., Ramírez-Iglesias, E., Reed, S.C., Rey, P.J., Reyes Gómez, V.M., Rodríguez, A., Rolo, V., Rubalcaba, J.G., Ruppert, J.C., Sala, O., Salah, A., Sebei, P.J., Stavi, I., Stephens, C., Teixido, A.L., Thomas, A.D., Throop, H.L., Tielbörger, K., Travers, S., Undrakhbold, S., Val, J., Valkó, O., Velbert, F., Wamiti, W., Wang, L., Wang, D., Wardle, G.M., Wolff, P., Yahdjian, L., Yari, R., Zaady, E., Zeberio, J.M., Zhang, Y., Zhou, X., Le Bagousse-Pinguet, Y., 2024. Unforeseen plant phenotypic diversity in a dry and grazed world. Nature 632, 808–814. https://doi.org/10.1038/s41586-024-07731-3.
Guuroh, R.T., Ruppert, J.C., Ferner, J., Čanak, K., Schmidtlein, S., Linstädter, A., 2018. Drivers of forage provision and erosion control in west African savannas - a macroecological perspective. Agric. Ecosyst. Environ. 251, 257–267. https://doi.org/10.1016/j.agee.2017.09.017.
Halbritter, A.H., de, Boeck, H.J., Eycott, A.E., Reinsch, S., Robinson, D.A., Vicca, S., Berauer, B., Christiansen, C.T., Estiarte, M., Grünzweig, J.M., Gya, R., Hansen, K., Jentsch, A., Lee, H., Linder, S., Marshall, J., Peñuelas, J., Kappel Schmidt, I., Stuart-Haëntjens, E., Wilfahrt, P., the ClimMani Working Group, Vandvik, V., 2020. The handbook for standardized field and laboratory measurements in terrestrial climate change experiments and observational studies (ClimEx). Methods Ecol. Evol. 11, 22–37. https://doi.org/10.1111/2041-210X.13331.
Herzog, F., Steiner, B., Bailey, D., Baudry, J., Billeter, R., Bukácek, R., de G., Blust, de R., Cock, Dirksen, J., Dormann, C.F., de R., Filippi, Frossard, E., Liira, J., Schmidt, T., Stöckli, R., Thenail, C., van Wingerden, W., Bugter, R., 2006. Assessing the intensity of temperate European agriculture at the landscape scale. Eur. J. Agron. 24, 165–181. https://doi.org/10.1016/j.eja.2005.07.006.
Iakunin, M., Taubert, F., Goss, R., Sasso, S., Feilhauer, H., Doktor, D., 2025. Grassland management and phenology affect trait retrieval accuracy from remote sensing observations. Eco. Inform. 87, 103068. https://doi.org/10.1016/j.ecoinf.2025.103068.
Jozdani, S.E., Johnson, B.A., Chen, D., 2019. Comparing deep neural networks, ensemble classifiers, and support vector machine algorithms for object-based urban land use/land cover classification. Remote Sens 11, 1713. https://doi.org/10.3390/rs11141713.
Kattenborn, T., Leitloff, J., Schiefer, F., Hinz, S., 2021. Review on convolutional neural networks (CNN) in vegetation remote sensing. ISPRS J. Photogramm. Remote Sens. 173, 24–49. https://doi.org/10.1016/j.isprsjprs.2020.12.010.
Kawamura, K., Nishigaki, T., Andriamananjara, A., Rakotonindrina, H., Tsujimoto, Y., Moritsuka, N., Rabenarivo, M., Razafimbelo, T., 2021. Using a one-dimensional convolutional neural network on visible and near-infrared spectroscopy to improve soil phosphorus prediction in Madagascar. Remote Sens 13, 1519. https://doi.org/10.3390/rs13081519.
Killeen, P., Kiringa, I., Yeap, T., Branco, P., 2024. Corn grain yield prediction using UAV-based high spatiotemporal resolution imagery, machine learning, and spatial cross-validation. Remote Sens 16, 683. https://doi.org/10.3390/rs16040683.
Knox, N.M., Skidmore, A.K., Schlerf, M., de, Boer, W.F., van Wieren, S.E., van der Waal, C., Prins, H.H.T., Slotow, R., 2010. Nitrogen prediction in grasses: effect of bandwidth and plant material state on absorption feature selection. Int. J. Remote Sens. 31, 691–704. https://doi.org/10.1080/01431160902895480.
Knox, N.M., Skidmore, A.K., Prins, H.H.T., Asner, G.P., van der Werff, H.M.A., de W. F., Boer, van der Waal, C., de H.J., Knegt, Kohi, E.M., Slotow, R., Grant, R.C., 2011. Dry season mapping of savanna forage quality, using the hyperspectral Carnegie airborne observatory sensor. Remote Sens. Environ. 115, 1478–1488. https://doi.org/10.1016/j.rse.2011.02.007.
Knox, N.M., Skidmore, A.K., Prins, H.H.T., Heitkönig, I.M.A., Slotow, R., van der Waal, C., de W.F., Boer, 2012. Remote sensing of forage nutrients: combining ecological and spectral absorption feature data. ISPRS J. Photogramm. Remote Sens. 72, 27–35. https://doi.org/10.1016/j.isprsjprs.2012.05.013.
Lee, M.A., 2018. A global comparison of the nutritive values of forage plants grown in contrasting environments. J. Plant Res. 131, 641–654. https://doi.org/10.1007/s10265-018-1024-y.
Lehnert, L.W., Meyer, H., Obermeier, W.A., Silva, B., Regeling, B., Bendix, J., 2019. Hyperspectral Data Analysis in R: The hsdar Package. 2019 89, p. 23. https://doi.org/10.18637/jss.v089.i12.
Lemaire, G., Hodgson, J., Chabbi, A., 2011. Grassland productivity and ecosystem services. Cabi International, London, ISBN 978-1-84593-809-3.
Liaw, A., Wiener, M., 2022. Classification and Regression by randomForest. R News.
Liu, E., Zhao, H., Zhang, S., He, J., Yang, X., Xiao, X., 2021a. Identification of plant species in an alpine steppe of northern Tibet using close-range hyperspectral imagery. Eco. Inform. 61, 101213. https://doi.org/10.1016/j.ecoinf.2021.101213.
Liu, N., Townsend, P.A., Naber, M.R., Bethke, P.C., Hills, W.B., Wang, Y., 2021b. Hyperspectral imagery to monitor crop nutrient status within and across growing seasons. Remote Sens. Environ. 255, 112303. https://doi.org/10.1016/j.rse.2021.112303.
Lorenzen, K., Vogt, J., Teuscher, M., Ostrowski, A., Thiele, J., 2024. Input Data of all Grassland Plots for Land-Use Intensity Index (LUI) Calculation Tool since 2006 - Revised 2023. Biodiversity Exploratories Information System.
Lyu, X., Li, X., Dang, D., Dou, H., Wang, K., Lou, A., 2022. Unmanned aerial vehicle (UAV) remote sensing in grassland ecosystem monitoring: a systematic review. Remote Sens 14, 1096. https://doi.org/10.3390/rs14051096.
Maestre, F.T., Le Bagousse-Pinguet, Y., Delgado-Baquerizo, M., Eldridge, D.J., Saiz, H., Berdugo, M., Gozalo, B., Ochoa, V., Guirado, E., García-Gómez, M., Valencia, E., Gaitán, J.J., Asensio, S., Mendoza, B.J., Plaza, C., Díaz-Martínez, P., Rey, A., Hu, H.-W., He, J.-Z., Wang, J.-T., Lehmann, A., Rillig, M.C., Cesarz, S., Eisenhauer, N., Martínez-Valderrama, J., Moreno-Jiménez, E., Sala, O., Abedi, M., Ahmadian, N., Alados, C.L., Aramayo, V., Amghar, F., Arredondo, T., Ahumada, R.J., Bahalkeh, K., Ben Salem, F., Blaum, N., Boldgiv, B., Bowker, M.A., Bran, D., Bu, C., Canessa, R., Castillo-Monroy, A.P., Castro, H., Castro, I., Castro-Quezada, P., Chibani, R., Conceição, A.A., Currier, C.M., Darrouzet-Nardi, A., Deák, B., Donoso, D.A., Dougill, A.J., Durán, J., Erdenetsetseg, B., Espinosa, C.I., Fajardo, A., Farzam, M., Ferrante, D., Frank, A.S.K., Fraser, L.H., Gherardi, L.A., Greenville, A.C., Guerra, C. A., Gusmán-Montalvan, E., Hernández-Hernández, R.M., Hölzel, N., Huber-Sannwald, E., Hughes, F.M., Jadán-Maza, O., Jeltsch, F., Jentsch, A., Kaseke, K.F., Köbel, M., Koopman, J.E., Leder, C.V., Linstädter, A., Le Roux, P.C., Li, X., Liancourt, P., Liu, J., Louw, M.A., Maggs-Kölling, G., Makhalanyane, T.P., Issa, O.M., Manzaneda, A.J., Marais, E., Mora, J.P., Moreno, G., Munson, S.M., Nunes, A., Oliva, G., Oñatibia, G.R., Peter, G., Pivari, M.O.D., Pueyo, Y., Quiroga, R.E., Rahmanian, S., Reed, S.C., Rey, P.J., Richard, B., Rodríguez, A., Rolo, V., Rubalcaba, J.G., Ruppert, J.C., Salah, A., Schuchardt, M.A., Spann, S., Stavi, I., Stephens, C.R.A., Swemmer, A.M., Teixido, A.L., Thomas, A.D., Throop, H.L., Tielbörger, K., Travers, S., Val, J., Valkó, O., van den Brink, L., Ayuso, S.V., Velbert, F., Wamiti, W., Wang, D., Wang, L., Wardle, G.M., Yahdjian, L., Zaady, E., Zhang, Y., Zhou, X., Singh, B.K., Gross, N., 2022. Grazing and ecosystem service delivery in global drylands. Science 378, 915–920. https://doi.org/10.1126/science.abq4062.
Männer, F.A., 2022. Hyperspectral reflection data for selected grassland EPs, 2020-2021. https://www.bexis.uni-jena.de.
Männer, F.A., Muro, J., Ferner, J., Dubovyk, O., Schmidtlein, S., Linstädter, A., 2025. Hyperspectral Reflection and Forage Data on Grassland Vegetation. https://doi.org/10.17632/dfyhrm5bw4.1.
Marino, S., Brugiapaglia, E., Miraglia, N., Persichilli, C., de M., Angelis, Pilla, F., Di Brita, A., 2024. Modelling of the above-ground biomass and ecological composition of semi-natural grasslands on the strenght of remote sensing data and machine learning algorithms. Eco. Inform. 82, 102740. https://doi.org/10.1016/j.ecoinf.2024.102740.
Melesse, A., Steingass, H., Boguhn, J., Rodehutscord, M., 2013. In vitro fermentation characteristics and effective utilisable crude protein in leaves and green pods of Moringa stenopetala and Moringa oleifera cultivated at low and mid-altitudes. Anim. Physiol. Nutr. 97, 537–546. https://doi.org/10.1111/j.1439-0396.2012.01294.x.
Menestrey Schwieger, D.A., Chambara F., Munyebvu –., Hamunyela, N., Tielbörger, K., Nesongano, W.C., Bilton, M.C., Bollig, M., Linstädter, A., 2025. Understanding rangeland desertification at the village level: a comparative study with a social-ecological systems perspective in Namibia. Hum. Ecol. https://doi.org/10.1007/s10745-025-00574-0.
Meng, X., Bao, Y., Wang, Y., Zhang, X., Liu, H., 2022. An advanced soil organic carbon content prediction model via fused temporal-spatial-spectral (TSS) information based on machine learning and deep learning algorithms. Remote Sens. Environ. 280, 113166. https://doi.org/10.1016/j.rse.2022.113166.
Menke, K.H., Steingass, H., 1988. Estimation of the energetic feed value obtained from chemical analysis and in vitro gas production using rumen fluid. Anim. Res. Develop. 28, 7–55.
Meyer, H., Pebesma, E., 2021. Predicting into unknown space? Estimating the area of applicability of spatial prediction models. Methods Ecol. Evol. 12, 1620–1633. https://doi.org/10.1111/2041-210X.13650.
Meyer, H., Lehnert, L.W., Wang, Y., Reudenbach, C., Nauss, T., Bendix, J., 2017. From Local Spectral Measurements to Maps of Vegetation Cover and Biomass on the Qinghai-Tibet-Plateau: Do we Need Hyperspectral Information?, 11 pp.
Meyer, H., Reudenbach, C., Wöllauer, S., Nauss, T., 2019. Importance of spatial predictor variable selection in machine learning applications – moving from data reproduction

to spatial prediction. Ecol. Model. 411, 108815. https://doi.org/10.1016/j.ecolmodel.2019.108815.
Meyer, S.N., Muro, J., Wöllauer, S., Schwarz, L.-M., Männer, F.A., Dubovyk, O., Linstädter, A., 2025. Land-use intensity effects on the biodiversity-ecosystem functioning relationship in semi-natural grasslands at management-relevant spatial scales. Landsc. Ecol. https://doi.org/10.1007/s10980-025-02186-x.
Michaud, A., Plantureux, S., Pottier, E., Baumont, R., 2015. Links between functional composition, biomass production and forage quality in permanent grasslands over a broad gradient of conditions. J. Agric. Sci. 153, 891–906. https://doi.org/10.1017/S0021859614000653.
Muro, J., Linstädter, A., Magdon, P., Wöllauer, S., Männer, F.A., Schwarz, L.-M., Ghazaryan, G., Schultz, J., Malenovský, Z., Dubovyk, O., 2022. Predicting plant biomass and species richness in temperate grasslands across regions, time, and land management with remote sensing and deep learning. Remote Sens. Environ. 282, 113262. https://doi.org/10.1016/j.rse.2022.113262.
Mutanga, O., Skidmore, A.K., 2004. Narrow band vegetation indices overcome the saturation problem in biomass estimation. Int. J. Remote Sens. 25, 3999–4014. https://doi.org/10.1080/01431160310001654923.
Naah, J.-B.S.N., Guuroh, R.T., Linstädter, A., 2017. Factors influencing local ecological knowledge of forage resources: ethnobotanical evidence from West Africa's savannas. J. Environ. Manag. 188, 297–307. https://doi.org/10.1016/j.jenvman.2016.11.064.
Näsi, R., Viljanen, N., Oliveira, R., Kaivosoja, J., Niemeläinen, O., Hakala, T., Markelin, L., Nezami, S., Suomalainen, J., Honkavaara, E., 2018. Optimizing radiometric processing and feature extraction of drone based hyperspectral frame format imagery for estimation of yield quantity and quality of a grass sward. Int. Arch. Photogramm. Remote Sens. Spatial Inf. Sci. XLII-3 1305–1310. https://doi.org/10.5194/isprs-archives-XLII-3-1305-2018.
Ng, W., Minasny, B., Jones, E., McBratney, A., 2022. To spike or to localize? Strategies to improve the prediction of local soil properties using regional spectral library. Geoderma 406, 115501. https://doi.org/10.1016/j.geoderma.2021.115501.
Niemeläinen, O., Kontturi, M., Jauhiainen, L., 2001. Estimated metabolizable energy yields of perennial and annual grass swards compared with those of spring barley and oat. AFSci 10, 335–346. https://doi.org/10.23986/afsci.5702.
Ningthoujam, R.K., Bloomfield, K.J., Crawley, M.J., Estrada, C., Prentice, I.C., 2025. Hyperspectral sensing of aboveground biomass and species diversity in a long-running grassland experiment. Eco. Inform. 86, 103028. https://doi.org/10.1016/j.ecoinf.2025.103028.
Obermeier, W.A., Lehnert, L.W., Pohl, M.J., Gianonni, S.M., Silva, B., Seibert, R., Laser, H., Moser, G., Muller, C., Luterbacher, J., Bendix, J., 2019. Grassland ecosystem services in a changing environment: the potential of hyperspectral monitoring. Remote Sens. Environ. 232, 16. https://doi.org/10.1016/j.rse.2019.111273.
Oliveira, R.A., Näsi, R., Niemeläinen, O., Nyholm, L., Alhonoja, K., Kaivosoja, J., Viljanen, N., Hakala, T., Nezami, S., Markelin, L., Jauhiainen, L., Honkavaara, E., 2019. Assessment of RGB and hyperspectral UAV remote sensing for grass quantity and quality estimation. Int. Arch. Photogramm. Remote. Sens. Spat. Inf. Sci. XLII-2/W13, 489–494. https://doi.org/10.5194/isprs-archives-XLII-2-W13-489-2019.
Oliveira, R.A., Näsi, R., Niemeläinen, O., Nyholm, L., Alhonoja, K., Kaivosoja, J., Jauhiainen, L., Viljanen, N., Nezami, S., Markelin, L., Hakala, T., Honkavaara, E., 2020. Machine learning estimators for the quantity and quality of grass swards used for silage production using drone-based imaging spectrometry and photogrammetry. Remote Sens. Environ. 246, 111830. https://doi.org/10.1016/j.rse.2020.111830.
Oliveira, R.A., Näsi, R., Korhonen, P., Mustonen, A., Niemeläinen, O., Koivumäki, N., Hakala, T., Suomalainen, J., Kaivosoja, J., Honkavaara, E., 2024. High-precision estimation of grass quality and quantity using UAS-based VNIR and SWIR hyperspectral cameras and machine learning. Precis. Agric. 25, 186–220. https://doi.org/10.1007/s11119-023-10064-2.
O'Malley, T., Bursztein, E., Long, J., Chollet, F., Jin, H., Invernizzi, L., 2019. Keras tuner. Retrieved May 21, 2020.
Omeer, A.A., Deshmukh, R.R., 2021. Improving the classification of invasive plant species by using continuous wavelet analysis and feature reduction techniques. Eco. Inform. 61, 101181. https://doi.org/10.1016/j.ecoinf.2020.101181.
van Oudtshoorn, F., 2016. Veld Management: Principles and Practices. Briza, Pretoria, 256 pp.
Padarian, J., Minasny, B., McBratney, A.B., 2019a. Transfer learning to localise a continental soil Vis-NIR calibration model. Geoderma 340, 279–288. https://doi.org/10.1016/j.geoderma.2019.01.009.
Padarian, J., Minasny, B., McBratney, A.B., 2019b. Using deep learning to predict soil properties from regional spectral data. Geoderma Reg. 16, e00198. https://doi.org/10.1016/j.geodrs.2018.e00198.
Pavlů, V., Hejcman, M., Pavlů, L., Gaisler, J., Nežerková, P., 2006. Effect of continuous grazing on forage quality, quantity and animal performance. Agric. Ecosyst. Environ. 113, 349–355. https://doi.org/10.1016/j.agee.2005.10.010.
Pi, W., Du, J., Bi, Y., Gao, X., Zhu, X., 2021. 3D-CNN based UAV hyperspectral imagery for grassland degradation indicator ground object classification research. Eco. Inform. 62, 101278. https://doi.org/10.1016/j.ecoinf.2021.101278.
Pinar, A., Curran, P.J., 1996. Technical note grass chlorophyll and the reflectance red edge. Int. J. Remote Sens. 17, 351–357. https://doi.org/10.1080/01431169608949010.
Pullanagari, R.R., Yule, I.J., Tuohy, M.P., Hedley, M.J., Dynes, R.A., King, W.M., 2012. In-field hyperspectral proximal sensing for estimating quality parameters of mixed pasture. Precis. Agric. 13, 351–369. https://doi.org/10.1007/s11119-011-9251-4.
Qi, Y., 2012. Random Forest for bioinformatics. In: Zhang, C., Ma, Y. (Eds.), Ensemble Machine Learning: Methods and Applications. Springer, US, Boston, MA, pp. 307–323.
R Core Team, 2018. R: A Language and Environment for Statistical Computing. R Foundation for Statistical Computing, Vienna, Austria, Vienna, Austria.
Reddersen, B., Fricke, T., Wachendorf, M., 2014. A multi-sensor approach for predicting biomass of extensively managed grassland. Comput. Electron. Agric. 109, 247–260. https://doi.org/10.1016/j.compag.2014.10.011.
Roy, D.P., Wulder, M.A., Loveland, T.R., W., C.E., Allen, R.G., Anderson, M.C., Helder, D., Irons, J.R., Johnson, D.M., Kennedy, R., Scambos, T.A., Schaaf, C.B., Schott, J.R., Sheng, Y., Vermote, E.F., Belward, A.S., Bindschadler, R., Cohen, W.B., Gao, F., Hipple, J.D., Hostert, P., Huntington, J., Justice, C.O., Kilic, A., Kovalskyy, V., Lee, Z.P., Lymburner, L., Masek, J.G., McCorkel, J., Shuai, Y., Trezza, R., Vogelmann, J., Wynne, R.H., Zhu, Z., 2014. Landsat-8: science and product vision for terrestrial global change research. Remote Sens. Environ. 145, 154–172. https://doi.org/10.1016/j.rse.2014.02.001.
Royimani, L., Mutanga, O., Odindi, J., Sibanda, M., Chamane, S., 2022. Determining the onset of autumn grass senescence in subtropical sour-veld grasslands using remote sensing proxies and the breakpoint approach. Eco. Inform. 69, 101651. https://doi.org/10.1016/j.ecoinf.2022.101651.
Ruppert, J.C., Linstädter, A., 2014. Convergence between ANPP estimation methods in grasslands – a practical solution to the comparability dilemma. Ecol. Indic. 36, 524–531. https://doi.org/10.1016/j.ecolind.2013.09.008.
Ruppert, J.C., Harmoney, K., Henkin, Z., Snyman, H.A., Sternberg, M., Willms, W., Linstädter, A., 2015. Quantifying drylands' drought resistance and recovery: the importance of drought intensity, dominant life history and grazing regime. Glob. Chang. Biol. 21, 258–1270. https://doi.org/10.1111/gcb.12777.
Sahoo, R.N., Rejith, R.G., Gakhar, S., Ranjan, R., Meena, M.C., Dey, A., Mukherjee, J., Dhakar, R., Meena, A., Daas, A., Babu, S., Upadhyay, P.K., Sekhawat, K., Kumar, S., Kumar, M., Chinnusamy, V., Khanna, M., 2024. Drone remote sensing of wheat N using hyperspectral sensor and machine learning. Precis. Agric. 25, 704–728. https://doi.org/10.1007/s11119-023-10089-7.
SASSCAL WeatherNet, 2020. SASSCAL WeatherNet - Okomumbonde (decomissioned) (Station ID: 113) - Monthly values. In: Southern African Science Service Centre for Climate Change and Adaptive Land Management. www.sasscalweathernet.org (accessed 18 January 2025).
Savitzky, A., Golay, M.J.E., 1964. Smoothing and differentiation of data by simplified least squares procedures. Anal. Chem. 36, 1627–1639. https://doi.org/10.1021/ac60214a047.
Schiefer, F., Schmidtlein, S., Frick, A., Frey, J., Klinke, R., Zielewska-Büttner, K., Junttila, S., Uhl, A., Kattenborn, T., 2023. UAV-based reference data for the prediction of fractional cover of standing deadwood from sentinel time series. ISPRS Open J. Photogrammetry Remote Sens. 8, 100034. https://doi.org/10.1016/j.ophoto.2023.100034.
Schweiger, A.K., Risch, A.C., Damm, A., Kneubühler, M., Haller, R., Schaepman, M.E., Schütz, M., 2015. Using imaging spectroscopy to predict above-ground plant biomass in alpine grasslands grazed by large ungulates. J. Veg. Sci. 26, 175–190. https://doi.org/10.1111/jvs.12214.
Shoko, C., Mutanga, O., Dube, T., 2016. Progress in the remote sensing of C3 and C4 grass species aboveground biomass over time and space. ISPRS J. Photogramm. Remote Sens. 120, 13–24. https://doi.org/10.1016/j.isprsjprs.2016.08.001.
Shwartz-Ziv, R., Armon, A., 2021. Tabular Data: Deep Learning Is Not all you Need.
Singh, L., Mutanga, O., Mafongoya, P., Peerbhay, K., 2017. Remote sensing of key grassland nutrients using hyperspectral techniques in KwaZulu-Natal, South Africa. J. Appl. Remote. Sens. 11, 36005.
Smith, C., Cogan, N., Badenhorst, P., Spangenberg, G., Smith, K., 2019. Field spectroscopy to determine nutritive value parameters of individual ryegrass plants. Agronomy 9, 293.
Smith, C., Karunaratne, S., Badenhorst, P., Cogan, N., Spangenberg, G., Smith, K., 2020. Machine learning algorithms to predict forage nutritive value of in situ perennial ryegrass plants using hyperspectral canopy reflectance data. Remote Sens 12, 928.
Soliveres, S., Smit, C., Maestre, F.T., 2015. Moving forward on facilitation research: response to changing environments and effects on the diversity, functioning and evolution of plant communities. Biol. Rev. 90, 297–313. https://doi.org/10.1111/brv.12110.
Squires, V.R., Dengler, J., Hua, L., Feng, H., 2018. Grasslands of the World: Diversity, Management and Conservation, 1st ed. CRC PRESS, Boca Raton.
Strohbach, B.J., 2014. Vegetation of the eastern communal conservancies in Namibia: I. Phytosociological descriptions. Koedoe 56. https://doi.org/10.4102/koedoe.v56i1.1116.
Suttie, J.M., Reynolds, S.G., Batello, C., 2005. Grasslands of the World. FAO, Rome.
Thenkabail, P.S., Lyon, J.G., 2012. Hyperspectral Remote Sensing of Vegetation. CRC Press, Boca Raton (Fla., 1 online resource).
Thenkabail, P.S., Smith, R.B., de, Pauw, E., 2000. Hyperspectral vegetation indices and their relationships with agricultural crop characteristics. Remote Sens. Environ. 71, 158–182. https://doi.org/10.1016/s0034-4257(99)00067-x.
Tirfessa, G., Tolera, A., 2020. Comparative evaluation of chemical composition, in vitro fermentation and methane production of selected tree forages. Agrofor. Syst. 94, 1445–1454. https://doi.org/10.1007/s10457-019-00391-7.
Tong, L., Liu, Y., Wang, Q., Zhang, Z., Li, J., Sun, Z., Khalifa, M., 2019. Relative effects of climate variation and human activities on grassland dynamics in Africa from 2000 to 2015. Eco. Inform. 53, 100979. https://doi.org/10.1016/j.ecoinf.2019.100979.
Utz, H.F., Melchinger, A.E., Seitz, G., Mistele, M., Zeddies, J., 1994. Economic aspects of breeding for yield and quality traits in forage maize. Plant Breed. 112, 110–119. https://doi.org/10.1111/j.1439-0523.1994.tb00658.x.
VDLUFA, 1976. Die chemische Untersuchung von Futtermitteln. In: VDLUFA-Verlag Darmstadt. Landwirtschaftlichen Versuchs-und Untersuchungsmethodik (VDLUFA-Methodenbuch), Band III, Germany. Handbuch der.

Vellinga, T.V., Andre, G., 1999. Sixty years of Dutch nitrogen fertiliser experiments, an overview of the effects of soil type, fertiliser input, management and of developments in time. NJAS 215–241. https://doi.org/10.18174/njas.v47i3.463.
Vidican, R., Mălinaș, A., Ranta, O., Moldovan, C., Marian, O., Ghețe, A., Ghișe, C.R., Popovici, F., Cătunescu, G.M., 2023. Using remote sensing vegetation indices for the discrimination and monitoring of agricultural crops: a critical review. Agronomy 13. https://doi.org/10.3390/agronomy13123040.
Wachendorf, M., Fricke, T., Moeckel, T., 2018. Remote sensing as a tool to assess botanical composition, structure, quantity and quality of temperate grasslands. Grass Forage Sci. 73, 1–14. https://doi.org/10.1111/gfs.12312.
Wang, Z., Ma, Y., Zhang, Y., Shang, J., 2022. Review of remote sensing applications in grassland monitoring. Remote Sens 14, 2903. https://doi.org/10.3390/rs14122903.
Wenger, S.J., Olden, J.D., 2012. Assessing transferability of ecological models: an underappreciated aspect of statistical validation. Methods Ecol. Evol. 3, 260–267. https://doi.org/10.1111/j.2041-210X.2011.00170.x.
Wengert, M., Wijesingha, J., Schulze-Brüninghoff, D., Wachendorf, M., Astor, T., 2022. Multisite and multitemporal grassland yield estimation using UAV-borne hyperspectral data. Remote Sens 14, 2068. https://doi.org/10.3390/rs14092068.
White, R.P., Murray, S., Rohweder, M., 2000. Grassland Ecosystems. World Resources Institute, Washington, DC.
Wolpert, D.H., Macready, W.G., 1997. No free lunch theorems for optimization. IEEE Trans. Evol. Computat. 1, 67–82. https://doi.org/10.1109/4235.585893.
World Bank Group, 2021. Climate Change Knowledge Portal. World Bank Group. https://climateknowledgeportal.worldbank.org/ (accessed 18 January 2025).
Wright, I.J., Reich, P.B., Westoby, M., Ackerly, D.D., Baruch, Z., Bongers, F., Cavender-Bares, J., Chapin, T., Cornelissen, J.H.C., Diemer, M., Flexas, J., Garnier, E., Groom, P.K., Gulias, J., Hikosaka, K., Lamont, B.B., Lee, T., Lee, W., Lusk, C., Midgley, J.J., Navas, M.-L., Niinemets, Ü., Oleksyn, J., Osada, N., Poorter, H., Poot, P., Prior, L., Pyankov, V.I., Roumet, C., Thomas, S.C., Tjoelker, M.G., Veneklaas, E.J., Villar, R., 2004. The worldwide leaf economics spectrum. Nature 428, 821–827. https://doi.org/10.1038/nature02403.
Xu, C., Holmgren, M., van Nes, E.H., Maestre, F.T., Soliveres, S., Berdugo, M., Kéfi, S., Marquet, P.A., Abades, S., Scheffer, M., 2015a. Can we infer plant facilitation from remote sensing? A test across global drylands. Ecol. Appl. 25, 1456–1462. https://doi.org/10.1890/14-2358.1.
Xu, C., van Nes, E.H., Holmgren, M., Kéfi, S., Scheffer, M., 2015b. Local facilitation may cause tipping points on a landscape level preceded by early-warning indicators. Am. Nat. 186, E81.
Xu, L., Saatchi, S.S., Yang, Y., Yu, Y., White, L., 2016. Performance of non-parametric algorithms for spatial mapping of tropical forest structure. Carbon Balance Manag. 11, 18. https://doi.org/10.1186/s13021-016-0062-9.
Xu, T., Han, B., Li, J., Du, Y., 2023. Domain-invariant feature and generative adversarial network boundary enhancement for multi-source unsupervised hyperspectral image classification. Remote Sens 15. https://doi.org/10.3390/rs15225306.
Yates, K.L., Bouchet, P.J., Caley, M.J., Mengersen, K., Randin, C.F., Parnell, S., Fielding, A.H., Bamford, A.J., Ban, S., Barbosa, A.M., Dormann, C.F., Elith, J., Embling, C.B., Ervin, G.N., Fisher, R., Gould, S., Graf, R.F., Gregr, E.J., Halpin, P.N., Heikkinen, R.K., Heinänen, S., Jones, A.R., Krishnakumar, P.K., Lauria, V., Lozano-Montes, H., Mannocci, L., Mellin, C., Mesgaran, M.B., Moreno-Amat, E., Mormede, S., Novaczek, E., Oppel, S., Ortuño Crespo, G., Peterson, A.T., Rapacciuolo, G., Roberts, J.J., Ross, R.E., Scales, K.L., Schoeman, D., Snelgrove, P., Sundblad, G., Thuiller, W., Torres, L.G., Verbruggen, H., Wang, L., Wenger, S., Whittingham, M.J., Zharikov, Y., Zurell, D., Sequeira, A.M.M., 2018. Outstanding challenges in the transferability of ecological models. Trends Ecol. Evol. 33, 790–802. https://doi.org/10.1016/j.tree.2018.08.001.
Zerbo, I., Bernhardt-Römermann, M., Ouédraogo, O., Hahn, K., Thiombiano, A., 2018. Diversity and occurrence of herbaceous communities in west African savannas in relation to climate, land use and habitat. Folia Geobot. 53, 17–39.
Zhang, T., Bi, Y., Du, J., Zhu, X., Gao, X., 2022. Classification of desert grassland species based on a local-global feature enhancement network and UAV hyperspectral remote sensing. Eco. Inform. 72, 101852. https://doi.org/10.1016/j.ecoinf.2022.101852.
Zhao, X., Wu, B., Xue, J., Shi, Y., Zhao, M., Geng, X., Yan, Z., Shen, H., Fang, J., 2023. Mapping forage biomass and quality of the Inner Mongolia grasslands by combining field measurements and Sentinel-2 observations. Remote Sens 15, 1973. https://doi.org/10.3390/rs15081973.
Zimmer, K., Amputu, V., Schwarz, L.-M., Linstädter, A., Sandhage-Hofmann, A., 2024. Soil characteristics within vegetation patches are sensitive indicators of savanna rangeland degradation in Central Namibia. Geoderma Reg. e00771. https://doi.org/10.1016/j.geodrs.2024.e00771.
Zomer, R.J., Xu, J., Trabucco, A., 2022. Version 3 of the global aridity index and potential evapotranspiration database. Sci Data 9, 409. https://doi.org/10.1038/s41597-022-01493-1.